A second visual rhodopsin gene, *rh1-2*, is expressed in zebrafish photoreceptors and found in other ray-finned fishes

James M. Morrow[1,2], Savo Lazic[3], Monica Dixon Fox[1], Claire Kuo[1], Ryan K. Schott[2], Eduardo de A. Gutierrez [2], Francesco Santini[6], Vincent Tropepe[1,4,5], and Belinda S. W. Chang[1,2,5]

[1]Department of Cell & Systems Biology
[2]Department of Ecology & Evolutionary Biology
[3]Department of Molecular Genetics
[4]Department of Ophthalmology & Vision Sciences
[5]Centre for the Analysis of Genome Evolution and Function
University of Toronto, Toronto, Canada

[6]Department of Ecology & Evolutionary Biology
University of California Los Angeles, Los Angeles, CA, USA

Corresponding Author:
Belinda Chang
Departments of Cell & Systems Biology/Ecology & Evolutionary Biology
University of Toronto
25 Harbord Street, Toronto, Ontario, M5S 3G5, Canada
T: 416-978-3507; E: belinda.chang@utoronto.ca

Keywords: rhodopsin, vision, gene duplication, zebrafish, teleost

Summary: While visual rhodopsin (*rh1*) is considered a single copy gene, the rhodopsin-like *rh1-2* has been maintained following duplication in groups of teleost fish and shares some functional features with rhodopsin.

ABSTRACT

Rhodopsin (*rh1*) is the visual pigment expressed in rod photoreceptors of vertebrates that is responsible for initiating the critical first step of dim-light vision. Rhodopsin is usually a single copy gene, however, we previously discovered a novel rhodopsin-like gene expressed in the zebrafish retina, *rh1-2*, which we identified as a functional photosensitive pigment that binds 11-*cis* retinal and activates in response to light. Here, we localize expression of *rh1-2* in the zebrafish retina to a subset of peripheral photoreceptor cells, which indicates a partially overlapping expression pattern with *rh1*. We also express, purify, and characterize Rh1-2, including investigations of the stability of the biologically active intermediate. Using fluorescence spectroscopy, we find the half-life of the rate of retinal release of Rh1-2 following photoactivation to be more similar to the visual pigment rhodopsin than to the non-visual pigment exo-rhodopsin (*exorh*), which releases retinal around 5 times faster. Phylogenetic and molecular evolutionary analyses show that *rh1-2* has ancient origins within teleost fishes, is under similar selective pressures to *rh1*, and likely experienced a burst of positive selection following its duplication and divergence from *rh1*. These findings indicate that *rh1-2* is another functional visual rhodopsin gene, which contradicts the prevailing notion that visual rhodopsin is primarily found as a single copy gene within ray-finned fishes. The reasons for retention of this duplicate gene, as well as possible functional consequences for the visual system, are discussed.

Journal of Experimental Biology • Advance article

INTRODUCTION

Vertebrate photoreception is mediated by opsins, which are members of the G protein-coupled receptor (GPCR) superfamily of proteins (Terakita, 2005). In the dark, opsins are covalently bound to a light-sensitive chromophore, 11-*cis* retinal, which acts as an inverse agonist to suppress dark state activation (Menon et al., 2001). When activated by light, the chromophore isomerizes to its all-*trans* conformation that initiates a signaling cascade within the cell (Baylor, 1996). Visual opsins are responsible for initiating the visual transduction cascade, while non-visual opsins are involved in processes such as circadian entrainment (Doyle et al., 2008) and the metabolism of retinal (Bellingham et al., 2003a), with some possibly contributing indirectly to image formation (Cheng et al., 2009). Rhodopsin is the visual opsin expressed in rod photoreceptors responsible for mediating dim-light vision in vertebrates (Nathans, 1992), and was the first GPCR to have its crystal structure resolved at high resolution (Palczewski et al., 2000).

While gene duplications have occurred multiple times in invertebrate opsins (Rivera et al., 2010; Serb et al., 2013) and vertebrate cone opsins (Hunt et al., 1998; Matsumoto et al., 2006), visual rhodopsin is generally considered to be a single copy gene, with only a few exceptions. Several eel species have two rhodopsins, one freshwater [*rh1fwo*] and one marine [*rh1dso*], where expression shifts from the former to the latter following migration during maturation (Beatty, 1975; Hope et al., 1998; Zhang et al., 2000; Zhang et al., 2002). Additionally, the short-fin pearleye [*Scopelarchus analis*], a deep-sea teleost, that also expresses an additional *rh1* gene, *rh1b*, in the accessory retina of adult fish after descending to greater ocean depths (Pointer et al., 2007). Other examples of multiple *rh1* genes are usually the result of species-specific duplication events (Lim et al., 1997). It is also interesting to note that the middle wavelength-sensitive cone opsin groups, which absorb similar wavelengths of light to rhodopsins, have been suggested to make greater contributions to adaptive vision through gene duplication (Gojobori and Innan, 2009).

Despite the scarcity of *rh1* gene duplications, zebrafish (*Danio rerio*) is a logical candidate for opsin gene duplication, considering most of its tissues are directly photoentrainable (Whitmore et al., 2000) and its array of nine visual opsins is a large

complement even among teleost fish (Chinen et al., 2003). Many non-visual opsins have been discovered in zebrafish through traditional sequencing studies, including five melanopsins (Bellingham et al., 2002; Davies et al., 2011), teleost multiple tissue [tmt] opsin (Moutsaki et al., 2003), two vertebrate ancient long [VAL] opsins (Kojima et al., 2008), and exo-rhodopsin (Mano et al., 1999). Additionally, a recent functional genomics screen identified 10 novel non-visual opsins (Davies et al., 2015). Meanwhile, the non-visual exo-rhodopsin (*exorh)*, expressed in the pineal gland of the brain and not in retinal photoreceptors, is not involved in vision, but is also orthologous to *rh1* of non-teleost vertebrates, with *rh1* in teleosts being the product of an ancient retrotransposition event that contains no introns (Fitzgibbon et al., 1995). This duplication is thought to have occurred no later than 284 million years ago, marking the onset of the radiation of ray-finned fish (Hurley et al., 2007), as basal Actinopterygians such as the sturgeon and gar also have intronless *rh1* genes (Bellingham et al., 2003b).

We previously identified another rhodopsin-like gene, *rh1-2*, in juvenile and adult zebrafish, but limited functional characterization prevented its classification as either a visual or non-visual opsin (Morrow et al., 2011). This novel gene was found to be expressed in the retina of adult zebrafish, but not in the brain. When regenerated with 11-*cis* retinal, Rh1-2 produced an absorption spectrum with a λ_{MAX} value of approximately 500 nm (Morrow et al., 2011), similar to both rhodopsin (Chinen et al., 2003) and exo-rhodopsin (Tarttelin et al., 2011). Orthologous sequences were also found in three other cyprinid fish, suggesting that *rh1-2* is not the result of a zebrafish-specific duplication event, and initial phylogenetic analyses hinted at a divergence from *rh1* during the earlier stages of teleost evolution (Morrow et al., 2011).

Here, we further characterize the expression and function Rh1-2 by comparing it to both rhodopsin and exo-rhodopsin in order to gain a better understanding of its role in photoreception and potential as a visual opsin. We localized *rh1-2* expression in the retina to a subset of peripheral photoreceptors, a pattern that partially overlaps *rh1* expression, but that is distinct from *exorh* expression in the pineal gland of the brain. When monitored following photoactivation using fluorescence spectroscopy, Rh1-2 was shown to release retinal at a rate comparable to rhodopsin and approximately five times

slower than exo-rhodopsin. Finally, *rh1-2* was identified in three additional species, including one outside of the family Cyprinidae, *Misgurnus anguillicaudatus*, and phylogenetic analyses show the *rh1-2* gene family is likely sister to ostariophysian *rh1* genes, having been subjected to purifying selection following duplication and divergence. This study adds new insights to visual system of zebrafish, and explores the implications of a second rhodopsin-like gene expressed in some teleost fish.

MATERIALS AND METHODS

Opsin sequences

RNA was extracted from adult eyes of various teleost fishes using the TRIzol reagent (Invitrogen, Carlsbad, CA, USA) and cDNA libraries were generated using the SMART cDNA Library Construction Kit (BD Biosciences, San Jose, CA, USA). Genomic DNA was extracted from various tissues of teleost fish using the DNeasy Blood & Tissue Kit (QIAGEN, Hilden, Germany). All specimens were euthanized prior to tissue extraction using an overdose of tricaine methane sulfonate (MS222, 300 mg/L; Sigma-Aldrich, St. Louis, MO, USA) buffered to neutral pH with sodium bicarbonate prior to fish immersion. Gene fragments of *rh1* and *rh1-2* were amplified from cDNA libraries and genomic DNA, respectively, using either previously designed *rh1-2* (Morrow et al., 2011) or acanthomorph *rh1* primers (Chen et al., 2003), with resulting bands being cloned into the pJET1.2 cloning vector (Fermentas, Waltham, MA, USA). Full length sequences of *rh1*, *rh1-2*, and *exorh*, were amplified from zebrafish eye (*rh1*, *rh1-2*) or brain (*exorh*) cDNA libraries. PCR was performed using PfuTurbo (Agilent, Santa Clara, CA, USA) with resulting bands being cloned into the p1D4-hrGFP II expression vector (Morrow and Chang, 2010). All vectors were sequenced using a 3730 DNA Analyzer (Applied Biosystems, Foster City, CA, USA).

In total, 19 new nucleotide sequences are introduced in this study, including 16 new *rh1* sequences (GenBank accession numbers: KY026025-KY026040) and 3 new *rh1-2* sequences (GenBank accession numbers: KY026041-KY026043) (Table S1). These sequences were combined with 117 rhodopsin gene sequences (*rh1*, *rh1-2*, *exorh*) obtained from GenBank in order to maintain even sampling across vertebrates within the limits of available data. Among these were four additional *rh1-2* genes not previously

studied, three from species of the *Sinocycloheilus* genus that were predicted as rhodopsin-like sequences from a recent cavefish genome project (Yang et al., 2016), and one that was extracted from the carp (*Cyprinus carpio*) genome. A second putative *rh1-2* sequence fragment was also identified within the carp genome, which is not unexpected due to a recent tetraploidization (Larhammar and Risinger, 1994), but was not included due to gaps in the first transmembrane domain. Four vertebrate *rh2* sequences were also obtained from GenBank and used as an outgroup. Sequences were aligned using the webPRANK (Löytynoja and Goldman, 2010) implementation of PRANK (Löytynoja and Goldman, 2005). Species list and accession numbers for all sequences used in the study are provided (Table S1).

In situ hybridization

Eyes were dissected from 21 and 175 dpf zebrafish (*Danio rerio*, Hamilton 1822), anesthetized with 160 mg/L of tricaine (ethyl 3-aminobenzoate methanesulfonate salt) (Sigma-Aldrich, St. Louis, MO, USA), then fixed in 4% paraformaldehye in phosphate-buffered saline (PBS) at 4°C overnight. Eyes were rinsed in PBS with 0.1% Tween-20 (PBT), then in methanol, before being stored in fresh methanol at -20°C. *In situ* hybridizations were performed on 3 dpf (control) and 5 dpf zebrafish embryos (whole mount), and eyes from 21 and 175 dpf zebrafish, as previously described (Wong et al., 2010). DIG-labeled RNA probes 700 bp in length, as well as unlabeled, full length blocking RNA from *rh1-2* (control), were amplified from *rh1* and *rh1-2* sequences inserted into the pBluescript cloning vector using T3 RNA Polymerase (Fermentas, Waltham, MA, USA). For our control using unlabeled *rh1-2* blocking RNA, the labeled *rh1* probe was pre-adsorbed with blocking RNA prior to *in situ* hybridization. A probe concentration of 1 ng/uL was using during the 70°C hybridization. Semi-thin plastic sections were made on 5 dpf embryos, where whole-mounts were rinsed with PBT, dehydrated using increasing concentrations of ethanol (from 30% to 90% in PBT), followed by 100% ethanol, and then embedded with increasing concentrations of Spurr's resin in ethanol (3:1, 1:1, 1:3). Samples were then left to polymerize at 65°C in 100% Spurr's resin. Semithin coronal sections were cut with a glass knife using an ultramicrotome and dried onto glass slides. Sections were 1.5 □m thick without counterstaining to maximize visualization. Cryosections were performed on 21 dpf and

175 dpf zebrafish eyes, which were washed 3 times in PBS, then put through a sucrose gradient at room temperature, 30 minutes per step: 5% sucrose in PBS, 2:1 5%:30%, 1:1 5%:30%, 1:2 5%:30%, with a final step in 30% sucrose in PBS at 4°C overnight. Eyes were incubated in 2:1 30% sucrose in PBS:Tissue-Tek OCT compound (VWR, Radnor, PA, USA) for 4 hours at room temperature, then 4°C overnight. Cryosections were performed at 20 μm on a Leica CM3050S cryostat, and collected on Superfrost Plus slides (VWR, Radnor, PA, USA) mounted in 90% glycerol/10% PBS. All images were taken on a Leica DM4500B compound microscope with a QIMAGING digital camera and OpenLab 4.0.2 software (Improvision, Coventry, UK).

Protein expression and spectroscopy

The p1D4-hrGFP II expression vector constructs containing full coding sequences of zebrafish *rh1*, *rh1-2*, and *exorh* were used to transiently transfect cultured HEK293T cells (ATCC CRL-11268) using Lipofectamine 2000 (Invitrogen, Carlsbad, CA, USA). Cells were harvested 48 h post-transfection and opsins were regenerated using 11-*cis* retinal, generously provided by Dr. Rosalie Crouch (Medical University of South Carolina). Visual pigments were solubilized in 1% N-dodecyl-β-D-maltoside (DM) and immunoaffinity purified with the 1D4 monoclonal antibody (University of British Columbia #95-062, Lot #1017; Molday and MacKenzie, 1983), as previously described (Morrow and Chang, 2010). Purified visual pigment samples were eluted in sodium phosphate buffer (50 mM NaPhos, 0.1% DM, pH 7). The ultraviolet-visible absorption spectra of purified opsin were recorded at 25°C using the Cary4000 double-beam spectrophotometer (Agilent, Santa Clara, CA, USA) and quartz absorption cuvettes (Helma, Paris, France). All λ_{MAX} values were calculated after fitting absorbance spectra to a standard template for A1 visual pigments (Govardovskii et al., 2000).

The protocol used to determine retinal release rates of visual pigments was modified from that of Farrens and Khorana (1995). Briefly, 0.05-0.20 μM visual pigment samples were incubated in sodium phosphate buffer (50 mM NaPhos, 0.1% DM, pH 7) at 20°C using submicro fluorometer cell cuvettes (Agilent, Santa Clara, CA, USA) and bleached for 30 seconds using a Fiber-Lite MI-152 Illuminator external light source (Dolan-Jenner, Boxborough, MA, USA), using a filter used to restrict wavelengths of light below 475 nm. Fluorescence measurements were integrated for 2 seconds at 30-second intervals using a Cary Eclipse fluorescence spectrophotometer, with temperature being maintained by a Cary Temperature Controller employing a Peltier Multicell Holder (Agilent, Santa Clara, CA, USA) and monitored by a temperature probe. The excitation wavelength was 295 nm (1.5 nm slit width) and the emission wavelength was 330 nm (10 nm slit width); no noticeable pigment bleaching by the excitation beam was detected. Retinal release was demonstrated through a sharp initial rise in intrinsic tryptophan fluorescence, representing a decrease in fluorescent quenching of W265 by the retinal chromophore. Data from the initial rise was fit to a three variable, first order exponential equation ($y = y_o + a(1-e^{-bx})$), with half-life values calculated based on the rate constant 'b' ($t_{1/2} = \ln 2/b$). All curve fitting resulted in r^2 values of greater than 0.9.

Phylogenetic and molecular evolutionary analyses

A maximum-likelihood rhodopsin gene tree was estimated in PhyML 3.0 (Guindon et al., 2010) under the GTR+I+G model using a BioNJ starting tree, the best of a NNI and SPR tree improvement, and 100 bootstraps. A Bayesian *rh1* gene tree was also constructed in MrBayes 3 (Ronquist and Huelsenbeck, 2003) using reversible jump MCMC with a gamma rate parameter (nst=mixed, rates=gamma), which explores the parameter space for the nucleotide model and the phylogenetic tree simultaneously. The analysis was run for five million generations with a 25% burn-in. Convergence was confirmed by checking that the standard deviations of split frequencies approached zero and that there was no obvious trend in the log likelihood plot.

To estimate the strength and form of selection acting on rhodopsin, the alignment, along with the maximum-likelihood gene tree, was analyzed with the codeml package of PAML 4 (Yang, 2007) using the random sites models (M0, M1a, M2a, M3, M7, M8a,

and M8), branch, branch-site model, and clade model C (CmC). Analyses were run on the complete *rh1* alignment and tree as well as two subsets, one pruned to only include ray-finned fish rhodopsin genes (including *exorh* as the outgroup) and the other pruned to contain only *rh1-2* (no outgroup).

Comparisons between the PAML random sites models were used to test for variation in ω (M3 vs M0) and for the presence of a positively selected class of sites (M2a vs M1a and M8 vs M7 and M8a). All analyses were run starting with the branch lengths estimated by PhyML repeated at least three times with varying initial starting points of κ(transition to transversion ratio) and $\omega$to avoid potential local optima. The model pairs were compared using a likelihood ratio test (LRT) with a $\chi 2$ distribution.

The branch, branch-site (Zhang et al., 2005) and clade models (CmC) (Bielawski and Yang, 2004) were used to test for changes in selective constraint and positive selection on the branch leading to the *rh1-2* clade and between the *rh1-2* clade and other rhodopsins. The branch model estimates a single omega value for each branch and/or clade type specified *a priori*. This model is useful for testing for overall changes in selective constraint between branches/clades. The branch-site and clade models allow $\omega$to vary both among sites and between branches/clades. The branch-site model has four site classes: 0) $0 < \omega_0 < 1$ for all branches; 1) $\omega_1 = 1$ for all branches, 2a) $\omega_{2a} = \omega_{2b} \geq 1$ in the foreground and $0 < \omega_{2a} = \omega_0 < 1$ in the background, and 2b) $\omega_{2b} = \omega_{2a} \geq 1$ in the foreground and $\omega_{2b} = \omega_1 = 1$ in the background. This model provides a test for positive selection on specified branches/clades and incorporates a Bayes' Empirical Bayes (BEB) analysis to identify codon sites under positive selection (Yang et al., 2005). CmC assumes that some sites evolve conservatively across the phylogeny (two classes of sites where $0 < \omega_0 < 1$ and $\omega_1 = 1$), while a class of sites is free to evolve differently among two or more partitions (e.g., $\omega_{D1} > 0$ and $\omega_{D1} \neq \omega_{D2} > 0$), which can be branches, clades, or a mix of both. Rather than a test for positive selection this provide a test for divergent selective pressure, although a test for positive selection can be performed if desired (see Chang et al., 2012). These models were applied only to the dataset pruned to contain only ray-finned fish rhodopsins.

RESULTS

rh1-2 is expressed in the outer nuclear layer of peripheral rod photoreceptors

We performed a series of *in situ* hybridizations to investigate the onset of *rh1-2* expression and to localize its expression in the retina. *In situ* hybridizations were performed using 700 bp coding sequence probes for both *rh1* and *rh1-2* in order to localize cellular expression in whole mount embryos 5 days post-fertilization (dpf), as well as both juvenile (21 dpf) and adult (175 dpf) eyes. At 5 dpf, expression of *rh1* was strongest in the peripheral retina, although some limited expression was also seen in the central retina (Fig. 1A), while *rh1-2* was only detected in a limited portion of the ventral peripheral retina (Fig. 1B). At 21 dpf, both *rh1* and *rh1-2* expression in the peripheral retina were more prominent relative to expression at 5 dpf (Fig. 1C and D). While the central retina contained more widespread *rh1* expression (Fig. 1E), there was no *rh1-2* expression (Fig. 1F). Expression at 175 dpf was similar to 21 dpf, with a strong *rh1* signal throughout the photoreceptor layer (Fig. 1G). Meanwhile, *rh1-2* was still localized to the ventral peripheral retina, with no staining shown in the central retina (Fig. 1H). Patterns of *rh1* expression were similar to those presented in previous studies (Raymond et al., 1995; Robinson et al., 1995; Takechi and Kawamura, 2005).

Expression of *rh1-2* was consistent with previous RT-PCR results that showed expression in 21 dpf juvenile fish and the adult retina but at significantly lower levels than *rh1* (Morrow et al., 2011). Furthermore, all expression of both *rh1* and *rh1-2* was confined to the outer nuclear layer (ONL), consisting of the cell bodies of rod and cone photoreceptors, suggesting that *rh1-2* protein expression occurs in photoreceptors as opposed to other retinal cells. Another interesting feature of *rh1-2* expression is that it often overlaps *rh1* expression, which suggests the possibility of co-expression of both genes in the same photoreceptor. Because of this overlap and since the nucleotide sequences of *rh1* and *rh1-2* share approximately 75% similarity, a sense-strand probe control experiment was run to exclude the possibility of cross-hybridization. The same 700 bp *rh1* probes were used to stain 3 dpf embryos both with and without the addition of full-length *rh1-2* blocking RNA, present at double the concentration of the *rh1* probe. The presence of the *rh1-2* blocking RNA did not have a significant effect on *rh1* staining,

Journal of Experimental Biology • Advance article

which suggests that there is likely no cross-hybridization occurring between *rh1*/*rh1-2* probes and their respective target transcripts (Fig. S1).

The λ_{MAX} of Rh1-2 is slightly blue-shifted compared to rhodopsin

Full-length gene sequences coding for zebrafish rhodopsin, Rh1-2, and exo-rhodopsin were inserted into the p1D4-hrGFP II expression vector (Morrow and Chang, 2010) and transiently transfected into HEK293T cells. All three pigments successfully bound 11-c*is* retinal, producing dark spectra with λ_{MAX} values of 500.6 ± 0.4 nm, 495.7 ± 0.3 nm, and 496.8 ± 0.5 nm for rhodopsin (n = 3), Rh1-2 (n = 3), and exo-rhodopsin (n = 3), respectively (Fig. 2). These values were consistent over three separate expression and with previous *in vitro* expression studies (Chinen et al., 2003; Morrow et al., 2011; Tarttelin et al., 2011). This shows that the λ_{MAX} of Rh1-2 is more similar to exo-rhodopsin than rhodopsin, but all three fall within the common range of ~500 nm, characteristic of most rhodopsins and many non-visual opsins (Kojima et al., 2000; Bowmaker, 2008).

Rh1-2 releases retinal at a rate similar to rhodopsin

We also measured the rate of release of all-*trans* retinal that occurs after photoactivation, requiring both hydrolysis of the Schiff base linkage between opsin and retinal, as well as dissociation of retinal from opsin. Using fluorescence spectroscopy, we measured the retinal release half-life of zebrafish rhodopsin as 6.5 ± 0.3 min (n = 6; Fig. 3), which is comparable to our previous results (Morrow and Chang, 2015). Despite much lower expression levels, Rh1-2 had a very similar retinal release half-life of 7.6 ± 0.8 min (n = 3; Fig. 3). Conversely, the non-visual exo-rhodopsin released retinal approximately five times faster than rhodopsin, with a half-life of 1.6 ± 0.3 min (n = 5; Fig. 3). This is the first time that retinal release has been measured in a non-visual opsin. These results show that the kinetics of photoactivation in Rh1-2 are more similar to rhodopsin than exo-rhodopsin, despite the fact that *in vitro* expression levels suggest that Rh1-2 may be less stable than both rhodopsin and exo-rhodopsin.

The *rh1-2* gene duplication occurred early in teleost fish evolution

Prior analyses lacked the taxonomic sampling to resolve the origins of *rh1-2*, although there were hints that it might be an ancient gene duplication in teleost fish (Morrow et al., 2011). Here, we amplified additional *rh1* and *rh1-2* sequences in order to better resolve

the evolutionary history of *rh1-2*, and its relationship to the *rh1* and *exorh* genes. Both maximum-likelihood and Bayesian phylogenetic analyses recovered with high bootstrap and posterior probability support, respectively, a single clade of *rh1-2* that was most closely related to anchovies and herring (Clupeomorpha) and ostariophysian fishes (Fig. 4, Fig. S2). Interestingly, the *rh1-2* clade was not most closely related to other duplicated ray-finned fish *rh1* genes, such as *exorh*, eel deep-sea rhodopsin (*dso*) and freshwater rhodopsin (*fwo*), or the pearleye *rh1a* and *rh1b*. The resulting topology largely recovered expected species relationships, particularly for major lineages, including the placement of lampreys and ray-finned fish (Hurley et al., 2007; Nakatani et al., 2011; Near et al., 2012). Interestingly, the two clades of eel *rh1* paralogs did not resolve into a monophyletic group, although this may have been due to unusual sequence evolution in nearby clades, which may be resolved with additional sequence data. Together, this suggests that the duplication that led to *rh1-2* occurred in the ancestor of a major group of bony fishes including anchovies, herrings and ostariophysian fishes (Ostarioclupeomorpha). Previous phylogenetic analysis of *rh1-2* found, with weak support, that *rh1-2* was sister to ostariophysians plus acanthomorphs (Morrow *et al.*, 2011). This discrepancy is likely due to the increased taxon sampling in the current study. These results further suggest that additional copies of *rh1-2* have yet to be identified from several groups of ray-finned fish. Additional sequences that become available as emerging genome projects of ostariophysian and clupeomorph fishes are annotated may help to further resolve the placement of this clade.

The *rh1-2* clade is under selective pressures similar to other *rh1* genes

Molecular evolutionary analyses were used to determine what changes in selective constraint occurred during and after the duplication that lead to *rh1-2*. Random sites models as implemented in PAML revealed that vertebrate rhodopsins as a whole were under strong selective constraint (average ω= 0.07, M0) (Table S2) with no evidence of positive selection (M2a vs M1a; M8 vs M8a, $p >> 0.5$ in all cases) (Table S2). Significant among-site rate variation was found, as would be expected for functional protein coding genes (M3 vs M0, $p < 0.00$) (Table S2). This was also true when only ray-finned fish were considered (ω= 0.08, M0; M2a vs M1a; M8 vs M8a, $p >> 0.5$ in all cases; M3 vs

M0, $p < 0.00$) (Table S2) and when only *rh1-2* was considered ($\omega = 0.09$, M0; M2a vs M1a; M8 vs M8a, $p >> 0.5$ in all cases; M3 vs M0, $p < 0.00$) (Table S2).

Accelerated evolution at a subset of sites may have accompanied the divergence of *rh1-2* from *rh1*

To further test for differences in selective constraint between *rh1-2* and other *rh1* genes, we used the branch-site, branch, and clade models on the dataset pruned to contain only ray-finned fish rhodopsin sequences. Using the branch-site model we observed increased positive selection on the branch leading to the *rh1-2* clade (Table S3), which approached significance when compared to the null model ($p = 0.071$), and identified a number of Bayes Empirical Bayes (BEB) sites with posterior probabilities above 0.8. Conversely, branch-site and clade model C (CmC) analyses with the *rh1-2* clade placed in the foreground found no evidence of either positive or divergent selection, supporting earlier random sites model results, which found that the *rh1-2* clade is under similar selective pressures as other *rh1* genes. Finally, the branch model was used to test for overall changes in selective constraint both on the branch leading to *rh1-2*, and on the entire clade. We found that the ωalong the branch and for the whole clade did not significantly differ from background ω($p >> 0.5$) (Tables S3, S4). This supports the hypothesis that *rh1-2* is a functional gene since it has been maintained under high levels of negative selection, corroborated by the M3 results that show significant rate variation. Together, these results suggest that *rh1-2* may have experienced a burst of positive selection following duplication and divergence from *rh1* and was later subject to purifying selection, which highlights an evolutionary path typical of genes that survive duplication and divergence events (Lynch and Conery, 2000).

DISCUSSION

Using *in situ* hybridization, along with both absorbance and fluorescence spectroscopy, we have shown that zebrafish *rh1-2* is expressed in peripheral photoreceptors of the retina and codes for a functional opsin protein that releases retinal at a similar rate to rhodopsin following photoactivation. However, *rh1-2* expression only starts around 5 dpf, and expresses weakly *in vitro*, both traits that are uncharacteristic of traditional *rh1* genes. Despite expressing at low levels, Rh1-2 has a similar half-life of retinal release to rhodopsin, while being almost 5 times greater than the non-visual exo-rhodopsin, suggesting the potential for a role in vision due to functional similarities to rhodopsin. Meanwhile, phylogenetic analyses place the *rh1-2* clade sister to ostariophysian and clupeomorph *rh1*, suggesting it originated following a fairly ancient duplication event, independent of other *rh1* duplications previously characterized in teleost fish. Here, we will discuss potential functional roles for *rh1-2* considering our findings, and the implications of this opsin gene for the zebrafish visual system.

The retinas of teleosts experience persistent neurogenesis in postembryonic fish, with new neurons arising from two different populations of stem cells. One are multipotent stem cells residing in the ciliary, or circumferential, marginal zone (CMZ), where progenitor cells give rise to Müller glia and all retinal neurons, except for rod photoreceptors, proliferating outward from the peripheral retina (Johns, 1977; Hitchcock et al., 2004; Stenkamp, 2007). The other are Müller glia cells, which give rise to rod precursor cells in the INL; once these rod precursors reach the outer nuclear layer (ONL), they divide and differentiate as rod photoreceptors (Bernardos et al., 2007; Nelson et al., 2008). Our *in situ* results show that expression of *rh1-2* is consistently located in the peripheral ONL of the retina, near the CMZ, but does not persist as cells are repositioned to a more central location in juvenile and adult fish. This suggests that *rh1-2* expression is limited to either rod photoreceptors derived from peripheral Müller glia cells that have recently emerged from the CMZ, or to cone photoreceptors recently derived from retinal progenitors of the CMZ that are still located in the periphery. Either possibility is consistent with the idea that *rh1-2* is more similar to visual opsins and expressed in retinal photoreceptors, as opposed to a non-visual opsin that can be expressed in other retinal cells, including horizontal cells (Cheng et al., 2009) and retinal ganglion cells

(Dacey et al., 2005; Panda et al., 2005), as well as in neural tissues outside of the retina, including the pineal (Mano et al., 1999), cerebellum (Blackshaw and Snyder, 1999), and spinal cord (Tartellin et al., 2003).

In order to function as a visual rhodopsin, *rh1-2* would be likely have to be expressed in rods, however expression in cones is also possible as there are rare cases where rhodopsins and cone opsins are expressed in the opposing photoreceptor type in reptiles and amphibians (Kojima et al., 1992; McDevitt et al., 1993; Schott et al., 2016). While a ~496 nm peak corresponding to Rh1-2 was not detected in previous microspectrophotometry studies that could have helped to localize expression at the cellular level (Nawrocki et al., 1985; Robinson et al., 1993; Cameron, 2002), this is likely due to either a lack of sensitivity to detect the poorly expressing opsin, or confounding signals with other opsins that have similar λ_{MAX} values, such as rhodopsin, Rh2-3 or Rh2-4 (Chinen et al., 2003). Interestingly, the expression pattern of *rh1-2* most resembles that of *rh2-3* and *rh2-4*, which is confined to peripheral photoreceptors near the CMZ in embryos and juveniles (Takechi and Kawamura, 2005). In adult fish, however, *rh2-3* and *rh2-4* expression expands to additional portions of the peripheral retina (Takechi and Kawamura, 2005), while the pattern of *rh1-2* stays mostly the same. It is possible that even limited *rh1-2* expression in the ventral peripheral retina, which produces a slightly blueshifted pigment compared to rhodopsin, may be advantageous for detecting the spectrum of downwelling light, a phenomenon that has been noted in cone opsin duplicates (Temple, 2011). Overall, the fact that *rh1-2* has both a different and more restrictive expression pattern than *rh1* in the retina is not unusual, as a diversity of expression patterns seem to be a common feature of duplicated opsin genes in teleost fish (Hofmann and Carleton, 2009).

Along with expression in the ONL, there are several functional features of the Rh1-2 protein that suggest it is likely to be a visual opsin gene. We previously reported that Rh1-2 successfully bound 11-*cis* retinal to form a functional pigment that activates in response to light, with a λ_{MAX} of approximately 500 nm (Morrow et al., 2011). Here, we present a more precise λ_{MAX} estimation of 495.7 ± 0.3 nm calculated via curve fitting to an A1 visual pigment template (Govardovskii et al., 2000). While this is ~5 nm blue shifted

Journal of Experimental Biology • Advance article

compared to rhodopsin, and more similar to exo-rhodopsin, all three pigments have λ_{MAX} values within the typical range of most vertebrate rhodopsins (Bowmaker, 2008). The ~4 nm blue shift of exo-rhodopsin relative to rhodopsin was suggested to be due to A124 (Tarttelin et al., 2011), since A124G substitutions in some deep-sea fish rhodopsins were associated with red-shifts of up to 3 nm (Hunt et al., 2001). Rh1-2 also has A124, suggesting the potential for a similar spectral tuning mechanism to exo-rhodopsin. However, the G124A substitution in zebrafish rhodopsin was recently shown to have no significant effect on spectral tuning (Morrow and Chang, 2015). While identical substitutions in different rhodopsin sequences can lead to variable shifts in spectral sensitivity, it is also possible that the blue-shift of Rh1-2 relative to rhodopsin is due to an accumulation of minor substitutions throughout its sequence, since no other differences were identified at sites known to be involved in rhodopsin spectral tuning (Yokoyama, 2000; Hunt et al., 2001).

Following photoactivation, Rh1-2 releases retinal at a rate similar to rhodopsin, suggesting that key structural aspects of rhodopsins, such as Schiff base stability and the hydrogen bond network of the chromophore binding pocket, are likely maintained in Rh1-2 (Janz and Farrens, 2004). This point is reflected in the significantly faster retinal release of cone visual pigments (Chen et al., 2012) and in our measurements of the non-visual exo-rhodopsin, which releases retinal almost 5 times faster following photoactivation. Because retinal release is a step in the retinoid cycle (Kiser et al., 2012), the metabolic cycle responsible for providing new 11-*cis* retinal molecules to regenerate free opsin, the slower retinal release of Rh1-2 also suggests that it may only have access to the retinal pigment epithelium-mediated pathway of retinal regeneration (Lamb and Pugh, 2004), and not the Müller cell-mediated pathway upon which cone opsins rely to help maintain rapid response kinetics (Wang et al., 2009; Wang and Kefalov, 2011). These results support the hypothesis that Rh1-2 is a visual opsin with rhodopsin-like functional properties.

An alternate hypothesis concerning the role of *rh1-2* is that it is a gene duplicate experiencing low levels of expression that has no unique functional role in photoreception. Where traditional rhodopsin genes maintain a high level of expression in the retina, the duplication event that gave rise to *rh1-2* failed to transfer the same regulatory elements that drive *rh1* expression (Kennedy et al., 2001), resulting in much lower expression levels. Additionally, *in vitro* expression of Rh1-2 suggests it is considerably less stable than rhodopsin. Despite having some characteristics of a redundant gene duplicate, this classification is usually attributed to genes resulting from relatively recent gene duplication events, with the vast majority of gene duplicates being silenced within a few million years (Lynch et al., 2001). However, unlike a more recent rhodopsin gene duplication, which may generate species-specific duplicates (Lim et al., 1997), our analyses suggest a much more ancient origin for the *rh1-2* gene, within the *rh1* gene family of a major group of bony fishes, which would place the duplication leading to the birth of *rh1-2* somewhere between 153 and 248 million years ago (Nakatani et al., 2011; Chen et al., 2013). PAML analyses also suggest the potential for increased evolutionary rates at a variety of sites along the branch leading to the *rh1-2* clade, followed by strong selective constraint characteristic of *rh1* genes within the *rh1-2* clade. This pattern of evolutionary rates is typical of genes that survive duplication and divergence events (Lynch and Conery, 2000), including retrogenes (Gayral et al., 2007). This pattern will likely become more significant when additional *rh1-2* sequences are discovered and included in future analyses.

Aside from *rh1-2*, only two other *rh1* gene duplications are known to have been retained in Actinopterigian fishes, making *rh1*, along with *sws1*, the least common opsin gene to experience duplication. The first example is from eels, which express the *rh1fwo* gene with the 11-*cis* 3,4-dehydroretinal (A2) chromophore in the early stages of life, where a red-shifted rhodopsin is thought to provide an advantage in the more long wavelength-shifted spectral environment of freshwater (Bridges, 1972; Loew, 1995). During maturation, eels migrate to a marine environment, with a more restricted and blue-shifted light spectrum, coupled with expression of a blue-shifted *rh1dso* gene, regenerated with 11-*cis* retinal (A1) chromophore (Hope et al., 1998; Zhang et al., 2000). This switch of both opsin and chromophore is a clear example of an adjustment of the visual system due

to a change in photic environment. Another example is the deep-sea pearleye, *Scoperlarchus analis*, which has a more traditional *rh1A* gene, along with *rh1B*, expressed alongside *rh1A* in adult fish living over 900 m below the surface (Pointer et al., 2007). The pearleye has unique cylindrical eye morphology, containing both a main retina, used for image formation, and an accessory retina, likely only capable of gross light perception (Collin et al., 1998), with *rh1B* expression being localized in this accessory retina (Pointer et al., 2007). Zebrafish does not experience an ontogenetic migration, possesses only A1 chromophore-based visual pigments (Allison et al., 2004), does not occupy deep-sea habitats, and does not have abnormal eye or retinal morphology, suggesting that it is unlikely for *rh1-2* to serve a similar function as the duplicated rhodopsin genes in either eels or the pearleye. This is supported by our phylogenetic analyses, which find *rh1fwo*, *rh1dso*, *rh1B*, and *rh1-2* all form distinct lineages that resulted from separate duplication and divergence events.

Perhaps the most intriguing result highlighted in this study is the partial overlapping expression patterns of *rh1* and *rh1-2*, suggesting the possibility that both genes may be co-expressed in a subset of photoreceptors, which could influence both the structure and function of these cells. Previous studies have hypothesized that cone opsin co-expression in humans could provide a developmental advantage (Xiao and Hendrickson, 2000). Alternatively, cone opsin co-expression in the cichlid fish, *Metriaclima zebra*, is thought to contribute to spectral tuning, although the λ_{MAX} differences in these opsins is 35 to 48 nm (Dalton et al., 2014), far exceeding the 5 nm difference between rhodopsin and Rh1-2. However, rhodopsin also serves an important structural role in rod photoreceptors, where it is packed into the outer segments and forms an array of dimers (Fotiadis et al., 2003). This arrangement could help to maximize the capacity of the rod outer segments, but likely also serves a functional purpose, with higher order rhodopsin oligomers being a more active species than monomers (Fotiadis et al., 2006). Considering the relatively low stability of Rh1-2 compared to rhodopsin, the incorporation of the former into a rhodopsin oligomer array could influence the structure of peripheral rod photoreceptors.

Co-expression of multiple *rh1* genes also raises the possibility of the formation of heterodimers, common in some GPCRs where it allows for differential binding between ligand and G protein (Waldhoer et al., 2005; Monnier et al., 2011). In fact, a functional dichotomy where one monomer responds to stimuli and the other binds the G protein was predicted for rhodopsin by molecular dynamics simulations (Neri et al., 2010), while alternative conformations for each monomer following activation could promote distinct functions from otherwise identical subunits (Jastrzebska et al., 2013). The presence of a rhodopsin/Rh1-2 heterodimer would likely influence the properties of a rod photoreceptor, however, further study is required to investigate this possibility. These studies will be challenging due to the low expression levels of *rh1-2* and its significant sequence similarity to the highly expressed *rh1*. Regardless, the potential of this interaction, as well as the presence of the *rh1-2* gene in other teleost fish should promote additional investigation into the influence of a second visual rhodopsin-like gene on the vertebrate visual system.

Acknowledgements

We acknowledge Dr. Rosalie Crouch for generously providing 11-*cis* retinal, and the CSB Imaging Facility at University of Toronto.

Competing Interests

The authors declare no competing or financial interests.

Author Contributions

JMM helped design the study, sequenced rhodopsin genes, expressed and characterized rhodopsins, and drafted the manuscript. SL helped design the study and performed *in situ* hybridization. MD and CK performed *in situ* hybridization. RKS and EAS ran the phylogenetic and selection analyses and provided text for the manuscript. FS contributed to the sequencing. VT helped design the study and provided guidance and edits for the manuscript. BSWC led study design, helped to draft the manuscript, and supervised all aspects of the project.

Funding

This work was supported by a National Sciences and Engineering Research Council Discovery Grant (BSWC) and a Vision Science Research Program Graduate Award (JMM).

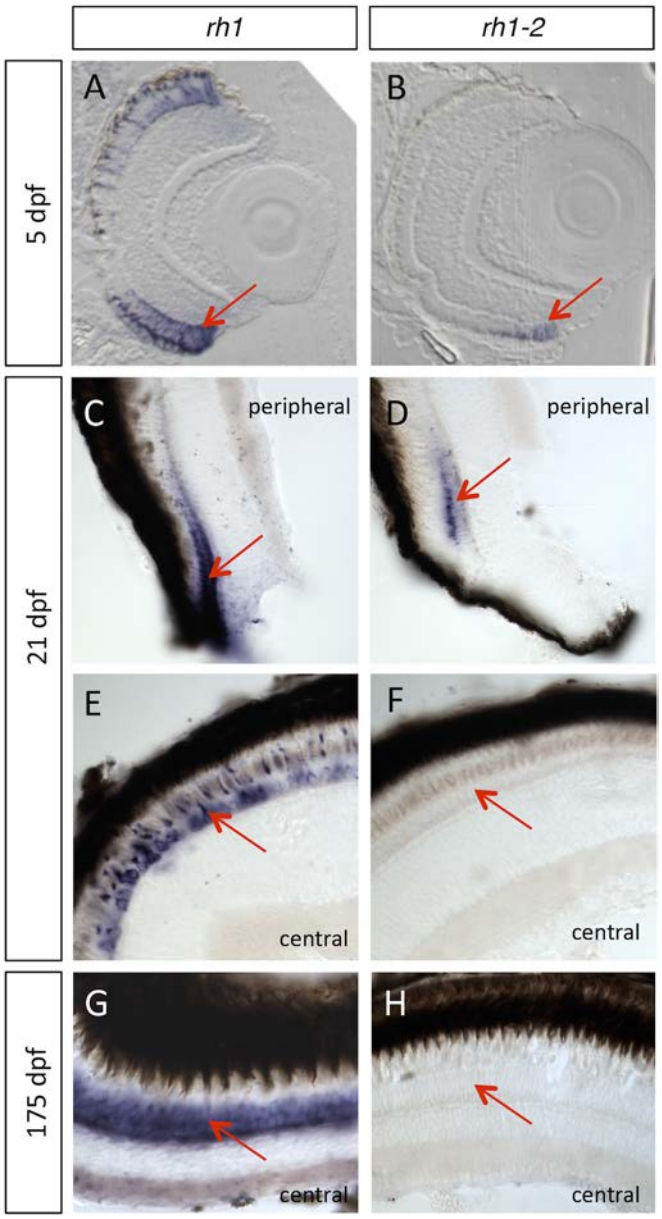

Figure 1. *In situ* hybridization (ISH) of *rh1-2* in the zebrafish retina at various developmental stages. (A-B) Whole mount ISH of 5 dpf embryos showing strong expression of *rh1* and weak expression of *rh1-2* in the ventral peripheral retina. **(C-F)** ISH of juvenile eyes at 21 dpf showing strong expression of *rh1* in both the central and peripheral retina, but weak only weak expression of *rh1-2* in the ventral peripheral retina. **(G-H)** ISH of adult eyes at 175 dpf showing strong expression of *rh1* in the central retina, but no signal from *rh1-2*. Both *rh1* and *rh1-2* also showed expression in the peripheral retinal at 175 dpf (results not shown). All expression of *rh1* and *rh1-2* was confined to the outer nuclear layer of the retina, consisting of the cell bodies of rod and cone photoreceptors. In all panels, the dorsal side is to the top and ventral is to the bottom.

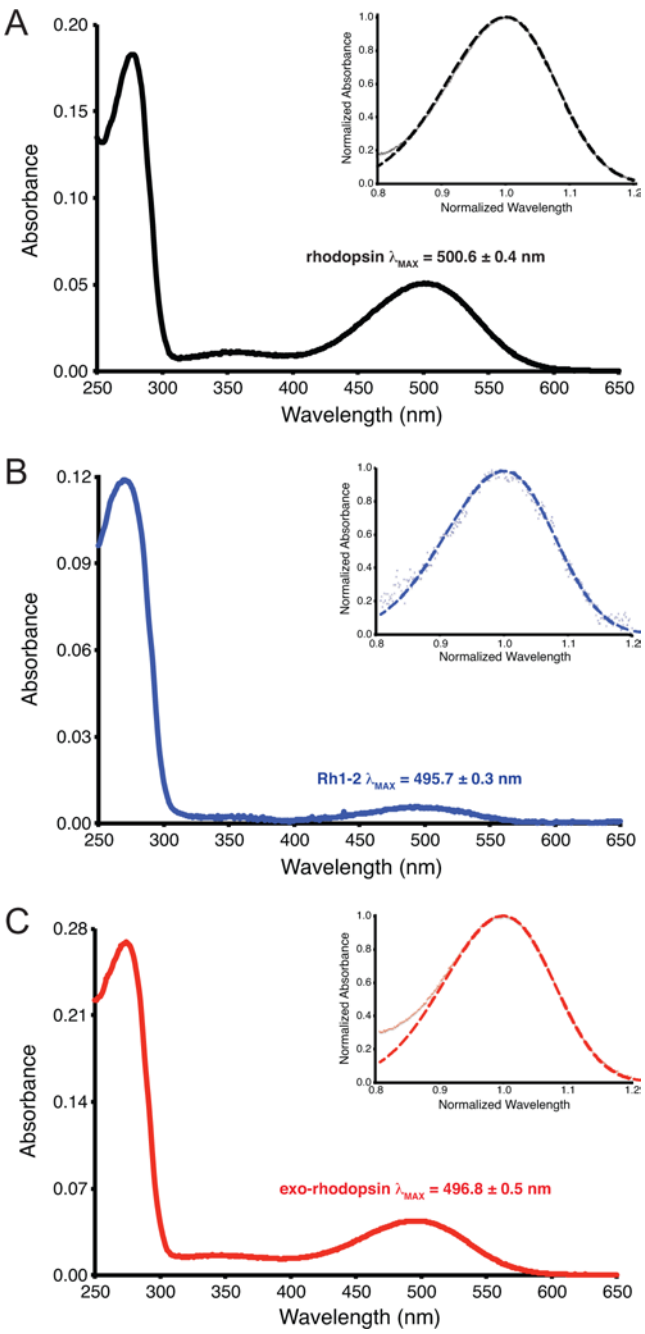

Figure 2. Absorbance spectra of zebrafish rhodopsins following *in vitro* expression and purification. Dark spectra of (A) zebrafish rhodopsin, (B) zebrafish Rh1-2, and (C) zebrafish exo-rhodopsin, along with respective curvefits to A1 visual pigment templates used to estimate λ_{MAX} (inset). Both Rh1-2 and exo-rhodopsin are slightly blue-shifted compared to rhodopsin. λ_{MAX} values represent the mean of three separate expressions for each pigment (n = 3) with standard deviations listed. Traces are shown for comparative purposes and are representative of these means.

Journal of Experimental Biology • Advance article

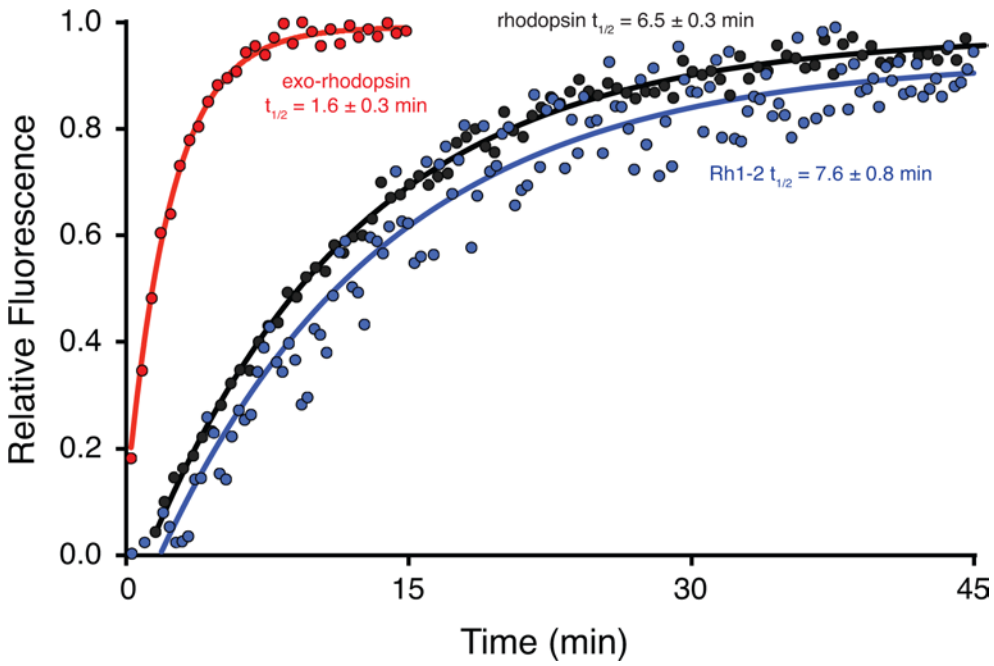

Figure 3. Retinal release rates of zebrafish rhodopsins at 20°C. The release of all-*trans* retinal is represented by an increase in fluorescence intensity following photoactivation of zebrafish rhodopsin (black), Rh1-2 (blue), and exo-rhodopsin (red). Half-life values are the mean of replicates (rhodopsin: n = 6; Rh1-2: n = 3; exo-rhodopsin n = 5) with standard deviations listed. Traces are shown for comparative purposes and are representative of these means.

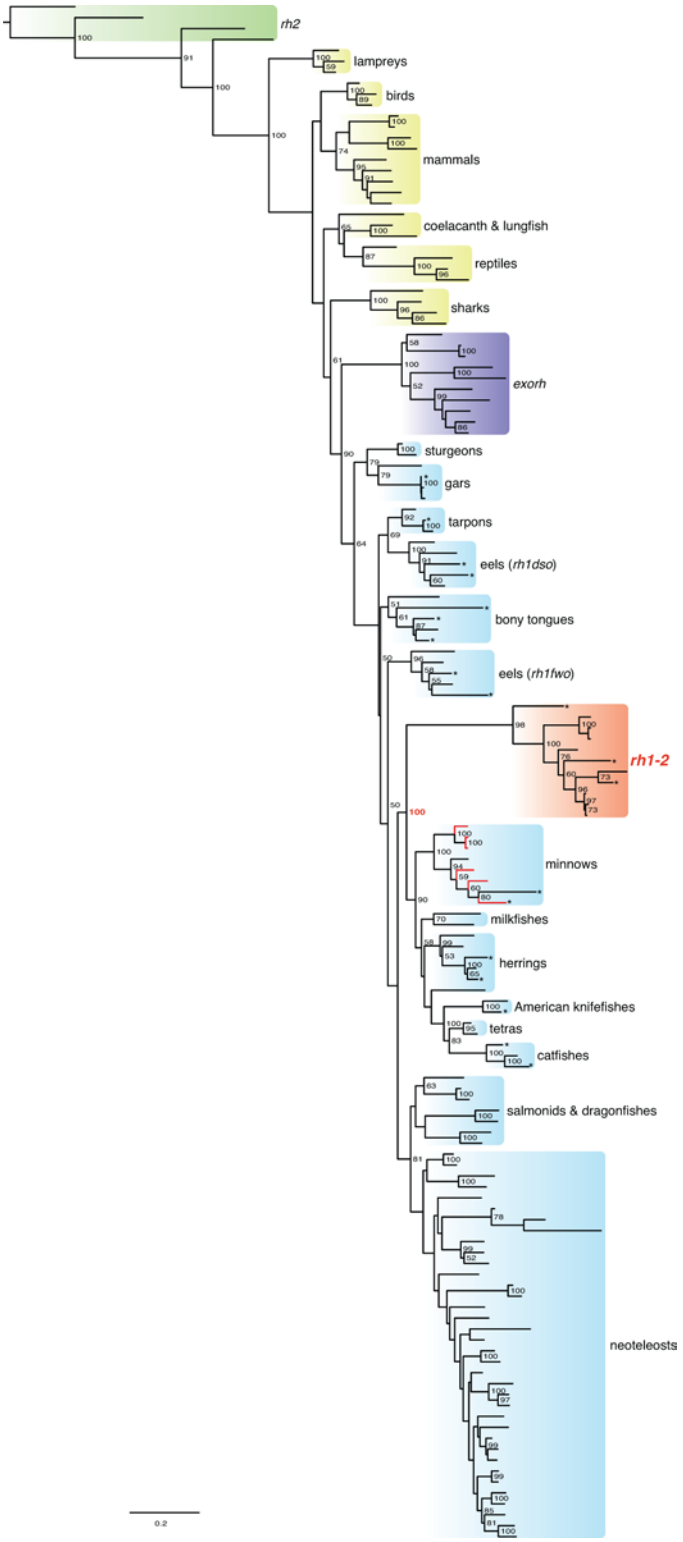

Figure 4. Maximum-likelihood phylogeny of vertebrate rhodopsin genes, including *rh1*, *rh1-2*, and *exorh*. The resulting topology mostly recovered expected relationships, including the positioning of lampreys and ray-finned fishes. Topology supports the

placement of the *rh1-2* gene family as the sister group to Ostarioclupeomorpha. Branches with asterisks represent sequences newly introduced in this study. Red branches in the minnows clade represent species that also have an *rh1-2* gene in this phylogeny. Several *rh2* opsin sequences were used as outgroups.

References

Allison, W. T., Haimberger, T. J., Hawryshyn, C. W. and Temple, S. E. (2004) Visual pigment composition in zebrafish: Evidence for a rhodopsin-porphyropsin interchange system. *Vis. Neurosci.* **21**, 945-952

Baylor, D. (1996) How photons start vision. *Proc. Natl. Acad. Sci. U.S.A.* **93,** 560-565

Beatty, D. D. (1975) Visual pigments of the American eel *Anguilla rostrata*. *Vision Res.* **15,** 771-776

Bellingham, J., Whitmore, D., Philip, A. R., Wells, D. J. and Foster, R. G. (2002) Zebrafish melanopsin: isolation, tissue localization and phylogenetic position. *Brain Res. Mol. Brain Res.* **107,** 128-136

Bellingham, J., Wells, D. J. and Foster, R. G. (2003a) *In silico* characterization and chromosomal localization of human RRH (peropsin) – implications for opsin evolution. *BMC Genomics* **4,** 3

Bellingham, J., Tarttelin, E. E., Foster, R. G. and Wells, D. J. (2003b) Structure and Evolution of the Teleost Extraretinal Rod-like Opsin (*errlo*) and ocular Rod Opsin (*rho*) Genes: Is Teleost *rho* a Retrogene? *J. Exp. Zool. B Mol. Dev. Evol.* **297,** 1-10

Bernardos, R. L., Berthel, L. K., Meyers, J. R. and Raymond, P. A. (2007) Late-stage neuronal progenitors in the retina are radial Müller glia that function as retinal stem cells. *J. Neurosci.* **27,** 7028-7040

Bielawski, J. P. and Yang, Z. (2004) A maximum likelihood method for detecting functional divergence at individual codon sites, with application to gene family evolution. *J. Mol. Evol.* **59,** 121-132

Blackshaw, S. and Snyder, S. H. (1999) Encephalopsin: A Novel Mammalian Extraretinal Opsin Discretely Localized in the Brain. *J. Neurosci.* **19,** 3681-3690

Bowmaker, J. K. (2008) Evolution of vertebrate visual pigments. *Vision Res.* **48,** 2022-2041

Bridges, C. D. (1972) The rhodopsin-porphyropsin visual system. In *Handbook of Sensory Physiology VII/1: Photochemistry of Vision* (ed. Dartnall H. J.), pp. 417-480. Springer-Verlag, Berlin

Cameron, D. A. (2002) Mapping absorbance spectra, cone fractions, and neuronal mechanisms to photopic spectral sensitivity in the zebrafish. *Vis. Neurosci.* **19,** 365-372

Chang, B. S., Du, J., Weadick, C. J., Müller, J., Bickelmann, C., Yu, D. D. and Morrow, J. M. (2012) The future of codon models in studies of molecular function: ancestral reconstruction and clade models of functional divergence. In *Codon Evolution: Mechanisms and Models* (ed. Cnnarozzi, G.M. and Schneider, A.), pp. 145-163. Oxford University Press Inc., New York.

Chen, W. J., Bonillo, C. and Lecointre G. (2003) Repeatability of clades as a criterion of reliability: a case study for molecular phylogeny of Acanthomorpha (Teleostei) with larger number of taxa. *Mol. Phylogenet. Evol.* **26,** 262-288

Chen, M. H., Kuemmel, C., Birge, R. R. and Knox, B. E. (2012) Rapid release of retinal from a cone visual pigment following photoactivation. *Biochemistry* **51,** 4117-4125

Chen, W. J., Lavoué, S. and Mayden, R. L. (2013) Evolutionary origin and early biogeography of otophysan fishes (Ostariophysi: Teleostei). *Evolution* **67,** 2218-2239

Cheng, N., Tsunenari, T. and Yau, K. W. (2009) Intrinsic light response of retinal horizontal cells of teleosts. *Nature* **460,** 899-903

Chinen, A., Hamaoka, T., Yamada, Y. and Kawamura, S. (2003) Gene duplication and spectral diversification of cone visual pigments of zebrafish. *Genetics* **163,** 663-675

Collin, S. P., Hoskins, R. V., Partridge, J. C. (1998) Seven retinal specializations in the tubular eye of the deep-sea pearleye, *Scopelarchus michaelsarsi*: a case study in visual optimization. *Brain Behav. Evol.* **51,** 291-314

Dacey, D. M., Liao, H. W., Peterson, B. B., Robinson, F. R., Smith, V. C., Pokorny, J., Yau, K. W. and Gamlin, P. D. (2005) Melanopsin-expressing ganglion cells in primate retina signal colour and irradiance and project to the LGN. *Nature* **433,** 749-754

Dalton, B. E., Lowe, E. R., Cronin, T. W. and Carleton, K. L. (2014) Spectral tuning by opsin coexpression in retinal regions that view different parts of the visual field. *Proc. Biol. Sci.* **281,** 20141980

Davies, W. I., Zheng, L., Hughes, S., Tamai, T. K., Turton, M., Halford, S., Foster, R. G., Whitmore, D. and Hankins, M. W. (2011) Functional diversity of melanopsins and their global expression in the teleost retina. *Cell Mol. Life Sci.* **68,** 4115-4132

Davies, W. I., Tamai, T. K., Zheng, L., Fu, J. K., Rihel, J., Foster, R. G., Whitmore, D. and Hankins, M. W. (2015) An extended family of novel vertebrate photopigments is widely expressed and displays a diversity of function. *Genome Res.* **25,** 1666-1679

Doyle, S. E., Yoshikawa, T., Hillson, H. and Menaker, M. (2008) Retinal pathways influence temporal niche. *Proc. Natl. Acad. Sci. U.S.A.* **105,** 13133-13138

Farrens, D. L. and Khorana, H. G. (1995) Structure and function in rhodopsin. Measurement of the rate of metarhodopsin II decay by fluorescence spectroscopy. *J. Biol. Chem.* **270,** 5073-5076

Fitzgibbon, J., Hope, A., Slobodynayuk, S. J., Bellingham, J., Bowmaker, J. K. and Hunt, D. M. (1995) The rhodopsin-encoding gene of bony fish lacks introns. *Gene* **164,** 273-277

Fotiadis, D., Liang, Y., Filipek, S., Saperstein, D. A., Engel, A. and Palczewski, K. (2003) Atomic-force microscopy: Rhodopsin dimers in native disc membranes. *Nature* **421,** 127-128

Fotiadis, D., Jastrzebska, B., Philippsen, A., Müller, D. J., Palczewski, K. and Engel, A. (2006) Structure of the rhodopsin dimer: a working model for G-protein-coupled receptors. *Curr. Opin. Struct. Biol.* **16,** 252-259

Gayral, P., Caminade, P., Boursot, P. and Galtier, N. (2007) The evolutionary fate of recently duplicated retrogenes in mice. *J. Evol. Biol.* **20,** 617-626

Gojobori, J. and Innan, H. (2009) Potential of fish opsin gene duplications to evolve new adaptive functions. *Trends Genet.* **25,** 198-202

Govardovskii, V. I., Fyhrquist, N., Reuter, T., Kuzmin, D. G. and Donner, K. (2000) In search of the visual pigment template. *Vis. Neurosci.* **17,** 509-528

Guindon, S., Dufayard, J-F., Lefort, V., Anisimova, M., Hordijk, W. and Gascuel, O. (2010) New algorithms and methods to estimate maximum-likelihood phylogenies: assessing the performance of PhyML 3.0. *Syst. Biol.* **59,** 307-321

Hitchcock, P., Ochocinska, M., Sieh, A. and Otteson, D. (2004) Persistent and injury-induced neurogenesis in the vertebrate eye. *Prog. Retin. Eye Res.* **23,** 183-194

Hofmann, C. M. and Carleton, K. L. (2009) Gene duplication and differential gene expression play an important role in the diversification of visual pigments in fish. *Integr. Comp. Biol.* **49,** 630-643

Hope, A. J., Partridge, J. C. and Haves, P. K. (1998) Switch in rod opsin gene expression in the European eel, *Anguilla anguilla* (L.). *Proc. Biol. Sci.* **265,** 869-874

Hunt, D. M., Dulai, K. S., Cowing, J. A., Julliot, C., Mollon, J. D., Bowmaker, J. K., Li, W. H. and Hewett-Emmett, D. (1998) Molecular evolution of trichromacy in primates. *Vision Res* **38,** 3299-3306

Hunt, D. M., Dulai, K. S., Partridge, J. C., Cottrill, P. and Bowmaker, J. K. (2001) The molecular basis for spectral tuning of rod visual pigments in deep-sea fish. *J. Exp. Biol.* **204,** 3333-3344

Hurley, I. A., Mueller, R. L., Dunn, K. A., Schmidt, E. J., Friedman, M., Ho, R. K., Prince, V. E., Yang, Z., Thomas, M. G. and Coates, M. I. (2007) A new time-scale for ray-finned fish evolution. *Proc. Biol. Sci.* **274,** 489-498

Janz, J. M. and Farrens, D. L. (2004) Role of the retinal hydrogen bond network in rhodopsin Schiff base stability and hydrolysis. *J. Biol. Chem.* **279,** 55886-55894

Jastrzebska, B., Orban, T., Golczak, M., Engel, A. and Palczewski, K. (2013) Asymmetry of the rhodopsin dimer in complex with transducin. *FASEB J.* **27,** 1572-1584

Johns, P. R. (1977) Growth of the adult goldfish eye. III. Source of the new retinal cells. *J. Comp. Neurol.* **176,** 343-357

Kennedy, B. N., Vihtelic, T. S., Checkley, L., Vaughan, K. T. and Hyde, D. R. (2001) Isolation of a zebrafish rod opsin promoter to generate a transgenic zebrafish line expressing enhanced green fluorescent protein in rod photoreceptors. *J. Biol. Chem.* **276,** 14037-14043

Kiser, P. D., Golczak, M., Maeda, A. and Palczewski, K. (2012) Key enzymes of the retinoid (visual) cycle in vertebrate retina. *Biochim. Biophys. Acta* **1821,** 137-151

Kojima, D., Okano, T., Fukada, Y., Shichida, Y., Yoshizawa, T. and Ebrey, T. G. (1992) Cone visual pigments are present in gecko rod cells. *Proc. Natl. Acad. Sci. U.S.A.* **89,** 6841-6845

Kojima, D., Mano, H. and Fukada, Y. (2000) Vertebrate ancient-long opsin: a green-sensitive photoreceptive molecule present in zebrafish deep brain and retinal horizontal cells. *J. Neurosci.* **20,** 2845-2851

Kojima, D., Torii, M., Fukada, Y. and Dowling, J. E. (2008) Differential expression of duplicated VAL-opsin genes in the developing zebrafish. *J. Neurochem.* **104,** 1364-1371

Lamb, T. D. and Pugh Jr., E. N (2004) Dark adaptation and the retinoid cycle of vision. *Prog. Retin. Eye Res.* **23,** 307-380

Larhammar, D. and Risinger, C. (1994) Molecular genetic aspects of tetraploidy in the common carp *Cyprinus carpio*. *Mol. Phylogenet. Evol.* **3,** 59-68
Lim, J., Chang, J. L. and Tsai, H. J. (1997) A second type of rod opsin cDNA from the common carp (*Cyprinus carpio*). *Biochim. Biophys. Acta* **1352,** 8-12
Loew, E. R. (1995) Determinants of visual pigment spectral location and photoreceptor cell spectral sensitivity. In *Neurobiology and Aspects of the Outer Retina* (ed. M.B.A. Djamgoz, S.N. Archer and S. Vallerga), pp.57-77. Chapman & Hall, London.
Löytynoja, A. and Goldman, N. (2005) An algorithm for progressive multiple alignment of sequences with insertions. *Proc. Natl. Acad. Sci. U.S.A.* **102,** 10557-10562
Löytynoja, A. and Goldman, N. (2010) webPRANK: a phylogeny-aware multiple sequence aligner with interactive alignment browser. *BMC Bioinformatics* **26,** 505
Lynch, M. and Conery, J. S. (2000) The evolutionary fate and consequences of duplicate genes. *Science* **290,** 1151-1155
Lynch, M., O'Helly, M., Walsh, B. and Force, A. (2001) The probability of preservation of a newly arisen gene duplicate. *Genetics* **159,** 1789-1804
Mano, H., Kojima, D. and Fukada, Y. (1999) Exo-rhodopsin: a novel rhodopsin expressed in the zebrafish pineal gland. *Mol. Brain Res.* **73,** 110-118
Matsumoto, Y., Fukamachi, S., Mitani, H. and Kawamura, S. (2006) Functional characterization of visual opsin repertoire in Medaka (*Oryzias latipes*). *Gene* **371,** 268-278
McDevitt, D. S., Brahma, S. K., Jeanny, J. C. and Hicks, D. (1993) Presence and foveal enrichment of rod opsin in the "all cone" retina of the American chameleon. *Anat. Rec.* **237,** 299-307
Menon, S. T., Han, M. and Sakmar, T. P. (2001) Rhodopsin: structural basis of molecular physiology. *Physiol. Rev.* **81,** 1659-1688
Molday, R. S. and MacKenzie, D. (1983) Monoclonal antibodies to rhodopsin: characterization, cross-reactivity, and applications as structural probes. *Biochemsitry* **22,** 653-660
Monnier, C., Tu, H., Bourrier, E., Vol, C., Lamarque, L., Trinquet, E., Pin, J. P. and Rondard, P. (2011) Trans-activation between 7TM domains: implication in heterodimeric GABAB receptor activation. *EMBO J.* **30,** 32-42
Morrow, J. M. and Chang, B. S. (2010) The p1D4-hrGFP II expression vector: a tool for expressing and purifying visual pigments and other G protein-coupled receptors. *Plasmid* **64,** 162-169
Morrow, J. M. and Chang, B. S. (2015) Comparative mutagenesis studies of retinal release in light-activated zebrafish rhodopsin using fluorescence spectroscopy. *Biochemistry* **54,** 4507-4518
Morrow, J. M, Lazic, S. and Chang, B. S. (2011) A novel rhodopsin-like gene expressed in zebrafish retina. *Vis. Neurosci.* **28,** 325-35
Moutsaki, P., Whitmore, D., Bellingham, J., Sakamoto, K., David-Gray, Z. K. and Foster, R. G. (2003) Teleost multiple tissue (tmt) opsin: a candidate photopigment regulating the peripheral clocks of zebrafish? *Brain Res. Mol. Brain Res.* **112,** 135-145
Nakatani, M., Miya, M., Mabuchi, K., Saitoh, K. and Nishida, M. (2011) Evolutionary history of Otophysi (Teleostei), major clade of the modern freshwater fishes: Pangaean origin and Mesozoic radiation. *BMC Evol. Biol.* **11,** 177
Nathans, J. (1992) Rhodopsin: structure, function, and genetics. *Biochemistry* **31,** 4923-4931
Nawrocki, L., BreMiller, R., Streisinger, G. and Kaplan, M. (1985) Larval and adult visual pigments of the zebrafish, *Brachydanio rerio*. *Vision Res.* **25,** 1569-1576
Near, T. J., Eytan, R. I., Dornburg, A., Kuhn, K. L., Moore, J. A., Davis, M. P., Wainwright, P. C., Friedman, M. and Smith, W. L. (2012) Resolution of ray-finned fish phylogeny and timing of diversification. *Proc. Natl. Acad. Sci. U.S.A.* **109,** 13698-13703
Nelson, S. M., Frey, R. A., Wardwell, S. L. and Stenkamp, D. L. (2008) The developmental sequence of gene expression within the rod photoreceptor lineage in embryonic zebrafish. *Dev. Dyn.* **237,** 2903-2917
Neri, M., Vanni, S., Tavernelli, I. and Rothelisberger, U. (2010) Role of aggregation in rhodopsin signal transduction. *Biochemistry* **49,** 4827-4832
Palczewski, K., Kumasaka, T., Hori, T., Behnke, C. A., Motoshima, H., Fox, B. A., Le Trong, I., Teller, D. C., Okada, T., Stenkamp, R. E., Yamamoto, M. and Miyano, M. (2000) Crystal structure of rhodopsin: A G protein-coupled receptor. *Science* **289,** 739-745
Panda, S., Nayak, S. K., Campo, B., Walker, J. R., Hogenesch, J. B. and Jegla, T. (2005) Illumination of the Melanopsin Signaling Pathway. *Science* **307,** 600-604

Pointer, M. A., Carvalho, J. S., Cowing, J. A., Bowmaker, J. K. and Hunt, D. M. (2007) The visual pigments of a deep-sea teleost, the pearl eye Scopelarchus analis. *J. Exp. Biol.* **210,** 2829-2835
Raymond, P. A., Barthel, L. K. and Curran, G. A. (1995) Developmental patterning of rod and cone photoreceptors in embryonic zebrafish. *J. Comp. Neurol.* **359,** 537-550
Rivera, A. S., Pankey, M. S., Plachetzki, D. C., Villacorta, C., Syme, A. E., Serb, J. M., Omilian, A. R. and Oakley, T. H. (2010) Gene duplication and the origins of morphological complexity in pancrustacean eyes, a genomic approach. *BMC Evol. Biol.* **10,** 123
Robinson, J., Schmitt, E. A., Hárosi, F. I., Reece, R. J. and Dowling, J. E. (1993) Zebrafish ultraviolet visual pigment: absorption spectrum, sequence, and localization. *Proc. Natl. Acad. Sci. U.S.A.* **90,** 6009-6012
Robinson, J., Schmitt, E. A. and Dowling, J. E. (1995) Temporal and spatial patterns of opsin gene expression in zebrafish (*Danio rerio*). *Vis. Neurosci.* **12,** 895-906
Ronquist, F. and Huelsenbeck, J. P. (2003) MrBayes 3: Bayesian phylogenetic inference under mixed models. *Bioinformatics* **19,** 1572-1574
Schott, R. K., Müller, J., Yang, C. G., Bhattacharyya, N., Chan, N., Xu, M., Morrow, J. M., Ghenu, A. H., Loew, E. R., Tropepe, V. and Chang, B. S. (2016) Evolutionary transformation of rod photoreceptors in the all-cone retina of a diurnal garter snake. *Proc. Natl. Acad. Sci. U.S.A.* **113,** 356-361
Serb, J. M., Porath-Krause, A. J. and Pairett, A. N. (2013) Uncovering a gene duplication of the photoreceptive protein, opsin, in scallops (Bivalvia: Pectinidae). *Integr. Comp. Biol.* **53,** 68-77
Stenkamp, D. L. (2007) Neurogenesis in the fish retina. *Int. Rev. Cytol.* **259,** 173-224
Takechi, M. and Kawamura, S. (2005) Temporal and spatial changes in the expression pattern of multiple red and green subtype opsin genes during zebrafish development. *J. Exp. Biol.* **208,** 1337-1345
Tarttelin, E. E., Bellingham, J., Hankins, M. W., Foster, R. G. and Lucas, R. J. (2003) Neuropsin (Opn5): a novel opsin identified in mammalian neural tissue. *FEBS Lett.* **554,** 410-416
Tarttelin, E. E., Fransen, M. P., Edwards, P. C., Hankins, M. W., Schertler, G. F., Vogel, R., Lucas, R. J. and Bellingham, J. (2011) Adaptation of pineal expressed teleost exo-rod opsin to non-image forming photoreception through enhanced Meta II decay. *Cell. Mol. Life Sci.* **68,** 3713-3723
Temple, S. E. (2011) Why different regions of the retina have different spectral sensitivities: A review of mechanisms and functional significance of intraretinal variability in spectral sensitivity in vertebrates. *Vis. Neurosci.* **28,** 281-293
Terakita, A. (2005) The opsins. *Genome Biol* **6,** 213
Waldhoer, M., Fong, J., Jones, R. M., Lunzer, M. M., Sharma, S. K., Kostenis, E., Portoghese, P. S. and Whistler, J. L. (2005) A heterodimer-selective agonist shows in vivo relevance of G protein-coupled receptor dimers. *Proc. Natl. Acad. Sci. U.S.A.* **102,** 9050-9055
Wang, J. S. and Kefalov, V. J. (2011) The cone-specific visual cycle. *Prog. Retin. Eye Res.* **30,** 115-128
Wang, J. S., Estevez, M. E., Cornwall, M. C. and Kefalov, V. J. (2009) Intra-retinal visual cycle required for rapid and complete cone dark adaptation. *Nat. Neurosci.* **12,** 295-302
Whitmore, D., Foulkes, N. S. and Sassone-Corsi, P. (2000) Light acts directly on organs and cells in culture to set the vertebrate circadian clock. *Nature* **404,** 87-91
Wong, L., Weadick, C. J., Kuo, C., Chang, B. S., Tropepe, V. (2010) Duplicate dmbx1 genes regulate progenitor cell cycle and differentiation during zebrafish midbrain and retinal development. *BMC Dev. Biol.* **10,** 100
Xiao, M. and Hendrickson, A. (2000) Spatial and temporal expression of short, long/medium, or both opsins in human fetal cones. *J. Comp. Neurol.* **425,** 545-559
Yang, Z. (2007) PAML 4: phylogenetic analysis by maximum likelihood. *Mol. Biol. Evol.* **24,** 1586-1591
Yang, Z., Wong, W. S. and Nielsen, R. (2005) Bayes empirical Bayes inference of amino acid sites under positive selection. *Mol. Biol. Evol.* **22,** 1107-1118
Yang, J., Chen, X., Bai, J., Fang, D., Qiu, Y., Jiang, W., Yuan, H., Bian, C., Lu, J., He, S. et al. (2016) The *Sinocycloheilus* cavefish genome provides insights into cave adaptations. *BMC Biol.* **14,** 1
Yokoyama, S. (2000) Molecular evolution of vertebrate visual pigments. *Prog. Retin. Eye Res.* **19,** 385-419
Zhang, H., Futami, K., Horie, N., Okamura, A., Utoh, T., Mikawa, N., Tanaka, S., Okamoto, N. and Oka, H. P. (2000) Molecular cloning of fresh water and deep-sea rod opsin genes from Japanese eel *Anguilla japonica* and expressional analyses during sexual maturation. *FEBS Lett.* **469,** 39-43

Zhang, H., Futami, K., Yamada, Y., Horie, N., Okamura, A., Utoh, T., Mikawa, N., Tanaka, S., Okamoto, N. and Oka, H. P. (2002) Isolation of freshwater and deep-sea type opsin genes from the common Japanese conger. *J. Fish Biol.* **61,** 313-324

Zhang, J., Nielsen, R. and Yang, Z. (2005) Evaluation of an improved branch-site likelihood method for detecting positive selection at the molecular level. *Mol. Biol. Evol.* **22,** 2472-2479

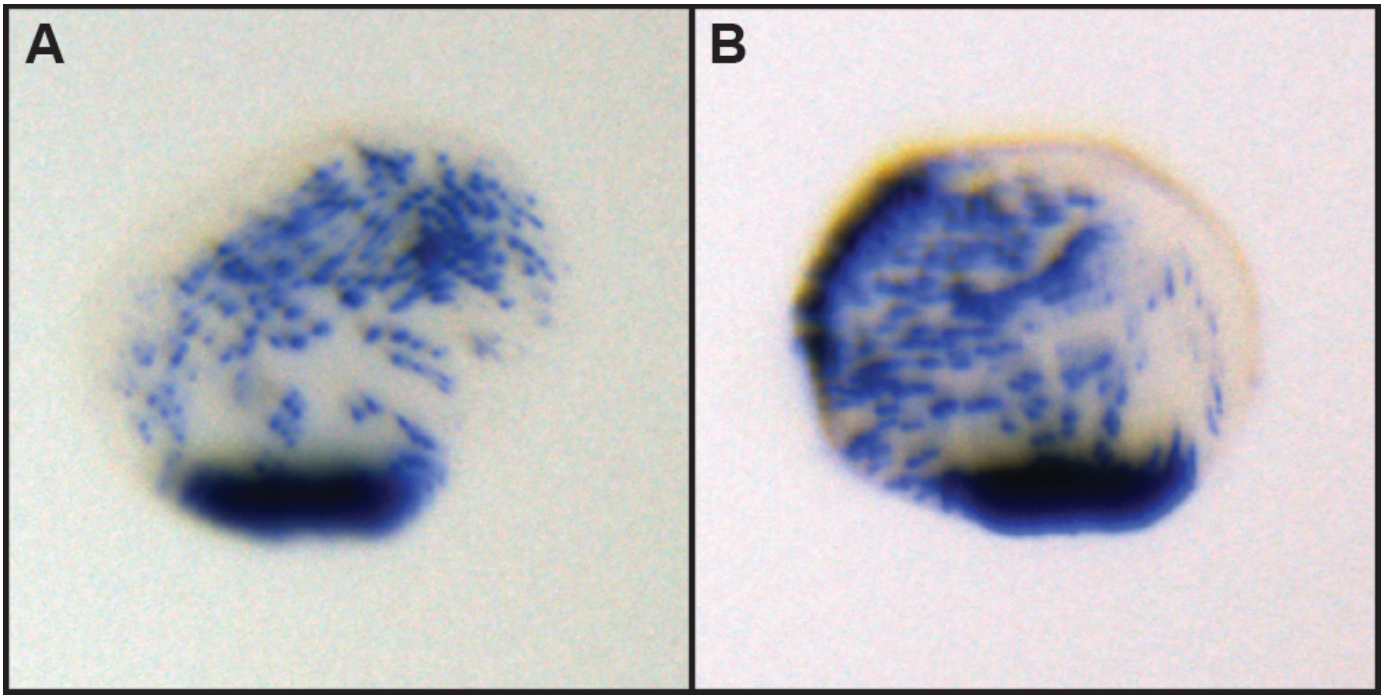

Figure S1. *In situ* hybridization of *rh1* in 3 dpf zebrafish embryos. Retinas from 3 dpf embryos were stained with the same 700 bp *rh1* probe used in all other experiments in this study both (A) with and (B) without the addition of full-length *rh1-2* blocking RNA, present at double the concentration of the rh1 probe. No significant difference in staining was detected.

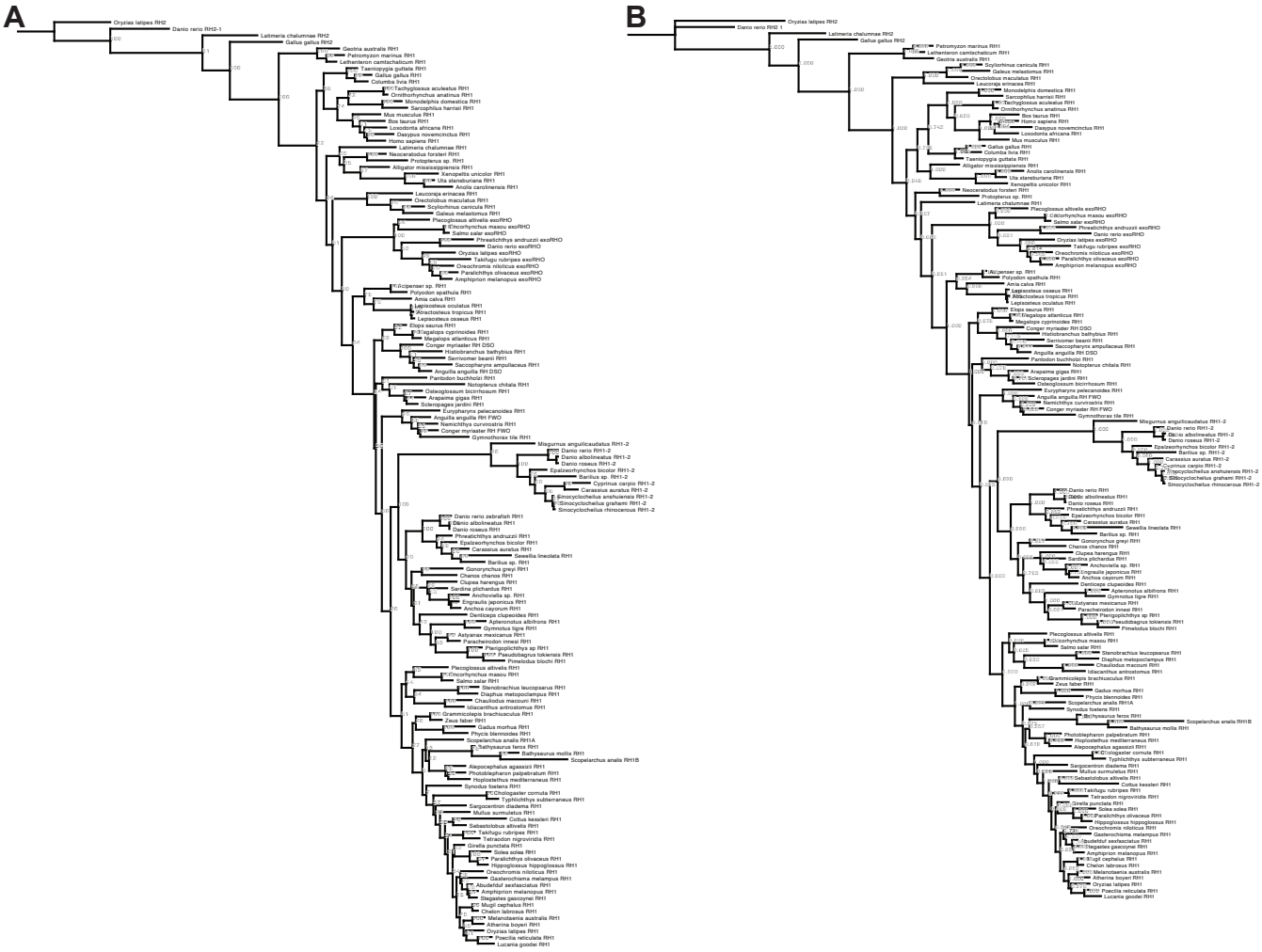

Figure S2. Detailed maximum-likelihood (A) and Bayesian phylogeny (B) of vertebrate rhodopsin genes. In both cases, high support was recovered for the placement of the *rh1-2* gene family as the sister group to Ostarioclupeomorpha. Several *rh2* opsin sequences were used as outgroups.

Table S1. List of sequences used in the phylogenetic and molecular evolutionary analyses of *rh1* genes.

Species Name	Common Name[1]	Gene	Accession/GI Number
Amphiprion melanopus	Fire clownfish	*exorh*	HM107820.1
Danio rerio	Zebrafish	*exorh*	71534272
Oncorhynchus masou	Masu salmon	*exorh*	478430872
Oreochromis niloticus	Nile tilapia	*exorh*	XM003438995.1
Oryzias latipes	Japanese medaka	*exorh*	XM004070540.1
Paralichthys olivaceus	Olive flounder	*exorh*	HM107825.1
Phreatichthys andruzzii	Cavefish	*exorh*	GQ404491.1
Plecoglossus altivelis	Ayu	*exorh*	28201134
Salmo salar	Atlantic salmon	*exorh*	185133057
Takifugu rubripes	Pufferfish	*exorh*	76362825
Anguilla anguilla	European eel	*rh1dso*	L78008.1
Conger myriaster	Whitespotted conger	*rh1dso*	12583666
Anguilla anguilla	European eel	*rh1fwo*	L78007.1
Conger myriaster	Whitespotted conger	*rh1fwo*	12583664
Abudefduf sexfasciatus	Scissortail sergeant	*rh1*	HQ286548.1
Acipenser sp.	Sturgeon	*rh1*	AF137206.1
Alepocephalus agassizii	Slickhead	*rh1*	JN544545.1
Alligator mississippiensis	American alligator	*rh1*	U23802.1
Amia calva	Bowfin	*rh1*	AF137208.1
Amphiprion melanopus	Fire clownfish	*rh1*	HM107824.1
Anchoa cayorum	Key anchovy marine	*rh1*	This study
Anchoviella sp.	Freshwater anchovy	*rh1*	This study
Anolis carolinensis	Carolina anole	*rh1*	XM003224879.1
Apteronotus albifrons	Black ghost knifefish	*rh1*	JN230983.1
Arapaima gigas	Arapaima	*rh1*	JN230972.1
Astyanax mexicanus	Mexican tetra	*rh1*	U12328.1
Atherina boyeri	Big-scale sand smelt	*rh1*	Y18676.1
Atractosteus tropicus	Tropical gar	*rh1*	JN230970.1
Barilius sp.	Barilius	*rh1*	This study
Bathysaurus ferox	Deepsea lizardfish	*rh1*	JN412585.1
Bathysaurus mollis	Highfin lizardfish	*rh1*	JN412586.1
Bos taurus	Cow	*rh1*	NM001014890.1
Carassius auratus	Golfish	*rh1*	L11863.1
Chanos chanos	Milfish	*rh1*	JN230981.1
Chauliodus macouni	Pacific viperfish	*rh1*	EU407250.1
Chelon labrosus	Thicklip grey mullet	*rh1*	Y18669.1
Chologaster cornuta	Swampfish	*rh1*	HQ729684.1
Clupea harengus	Atlantic herring	*rh1*	XM_012826141.1
Columba livia	Pigeon	*rh1*	4887218-4887219
Cottus kessleri	Kesslers sculpin	*rh1*	L42953.1
Danio albolineatus	Pearl danio	*rh1*	JQ614122.1

Danio rerio	Zebrafish	*rh1*	18859316:
Danio roseus	Rose danio	*rh1*	JQ614148.1
Dasypus novemcinctus	Armadillo	*rh1*	XM004477246.1
Denticeps clupeoides	Denticle herring	*rh1*	JN230976.1
Diaphus metopoclampus	Spothead lantern fish	*rh1*	JN544536.1
Elops saurus	Ladyfish	*rh1*	JN230971.1
Engraulis japonicus	Japanese anchovy	*rh1*	AB731902.1
Epalzeorhynchos bicolor	Redtailed black shark	*rh1*	HQ286332.1
Eurypharynx pelecanoides	Pelican eel	*rh1*	JN544544.1
Gadus morhua	Atlantic cod	*rh1*	AF385832.1
Galeus melastomus	Blackmouth catshark	*rh1*	Y17586.1
Gallus gallus	Chicken	*rh1*	NM001030606.1
Gasterochisma melampus	Butterfly kingfish	*rh1*	DQ882021.1
Geotria australis	Pouched lamprey	*rh1*	AY366493.1
Girella punctata	Largescale blackfish	*rh1*	AB158262.3
Gnorhynchus greyi	Beaked salmon	*rh1*	EU409632
Grammicolepis brachiusculus	Thorny tinselfish	*rh1*	EU637964.1
Gymnothorax tile	Moray eel	*rh1*	This study
Gymnotus tigre	Tiger knifefish	*rh1*	This study
Hippoglossus hippoglossus	Atlantic halibut	*rh1*	AF156265.1
Histiobranchus bathybius	Deepwater arrowtooth eel	*rh1*	JN544542.1
Homo sapiens	Human	*rh1*	169808383
Hoplostethus mediterraneus	Mediterranean slimehead	*rh1*	JN412583.1
Idiacanthus antrostomus	Pacific blackdragon	*rh1*	EU407249.1
Latimeria chalumnae	Coelacanth	*rh1*	4836673-4836677
Lepisosteus oculatus	Spotted gar	*rh1*	This study
Lepisosteus osseus	Longnose gar	*rh1*	AF137207.1
Lethenteron camtschaticum	Artic lamprey	*rh1*	46917273
Leucoraja erinacea	Little skate	*rh1*	U81514.1
Loxodonta africana	Elephant	*rh1*	344275992
Lucania goodei	Bluefin killifish	*rh1*	AY296738.1
Megalops atlanticus	Atlantic tarpon	*rh1*	AY158050
Megalops cyprinoides	Indo-Pacific tarpon	*rh1*	This study
Melanotaenia australis	Western rainbowfish	*rh1*	FJ940704.1
Monodelphis domestica	Short-tailed opossum	*rh1*	XM001366188.1
Mugil cephalus	Flathead mullet	*rh1*	4210736
Mullus surmuletus	Striped red mullet	*rh1*	4210732
Mus musculus	Mouse	*rh1*	NM_145383.1
Nemichthys curvirostris	Boxer snipe eel	*rh1*	This study
Neoceratodus forsteri	Lungfish	*rh1*	EF526295.1
Notopterus chitala	Clown knifefish	*rh1*	This study
Oncorhynchus masou	Masu salmon	*rh1*	478430870
Orectolobus maculatus	Spotted wobbegong	*rh1*	JX534163.1
Oreochromis niloticus	Niles tilapia	*rh1*	348502996
Ornithorhynchus anatinus	Platypus	*rh1*	NM001127627.1

Oryzias latipes	Japanese medaka	*rh1*	66796119
Osteoglossum bicirrhosum	Silver arowana	*rh1*	This study
Pantodon buchholzi	Freshwater butterflyfish	*rh1*	AF137210.1
Paracheirodon innesi	Neon tetra	*rh1*	84095053
Paralichthys olivaceus	Olive flounder	*rh1*	HQ413772.1
Petromyzon marinus	Sea lamprey	*rh1*	1513320-1513324
Photoblepharon palpebratum	Eyelightfish	*rh1*	EU637993.1
Phreatichthys andruzzii	Cavefish	*rh1*	JQ413240.1
Phycis blennoides	Greater forkbeard	*rh1*	JN412579.1
Pimelodus blochim	Blochs catfish	*rh1*	This study
Plecoglossus altivelis	Ayu	*rh1*	19912833
Poecilia reticulata	Guppy	*rh1*	DQ912024.1
Polyodon spathula	American paddlefish	*rh1*	AF369050.1
Protopterus sp.	African lungfish	*rh1*	AF369054.1
Pseudobagrus tokiensis	Balgrid	*rh1*	FJ197075.1
Pterigoplichthys sp.	Armored catfish	*rh1*	This study
Saccopharynx ampullaceus	Gulper eel	*rh1*	This study
Salmo salar	Atlantic salmon	*rh1*	185133085
Sarcophilus harrisii	Tasmian devil	*rh1*	395516643
Sardina pilchardus	Sardine	*rh1*	Y18677.1
Sargocentron diadema	Crown squirrelfish	*rh1*	U57537.1
Scleropages jardini	Gulf saratoga	*rh1*	This study
Scyliorhinus canicula	Small-spotted catshark	*rh1*	3256019
Sebastolobus altivelis	Longspine thornyhead	*rh1*	DQ490124.1
Serrivomer beanii	Sawtooth eel	*rh1*	This study
Sewellia lineolata	Tiger hillstream loach	*rh1*	This study
Solea solea	Common sole	*rh1*	4210866
Stegastes gascoynei	Coral Sea gregory damselfish	*rh1*	HQ286557.1
Stenobrachius leucopsarus	Northern lampfish	*rh1*	EU407251.1
Synodus foetens	Inshore lizardfish	*rh1*	JN231001.1
Tachyglossus aculeatus	Echidna	*rh1*	398018454
Taeniopya guttata	Zebra finch	*rh1*	115529257
Takifugu rubripes	Pufferfish	*rh1*	118344635
Tetraodon nigroviridis	Green spotted puffer	*rh1*	AJ293018.1
Typhlichthys subterraneus	Southern cavefish	*rh1*	HQ729699.1
Uta stansburiana	Side-blotched lizard	*rh1*	DQ100323.1
Xenopeltis unicolor	Sunbeam snake	*rh1*	FJ497233.1
Zeus faber	John dory	*rh1*	Y14484.1
Barilius sp.	Barilius	*rh1-2*	This study
Carassius auratus	Goldfish	*rh1-2*	This study
Cyprinus carpio	Common carp	*rh1-2*	Extracted from genome
Danio albolineatus	Pearl danio	*rh1-2*	HQ286328
Danio rerio	Zebrafish	*rh1-2*	HQ286326
Danio roseus	Rose danio	*rh1-2*	HQ286327
Epalzeorhynchos bicolor	Redtailed black shark	*rh1-2*	HQ286329

Misgurnus anguilicaudatus	Dojo loach	*rh1-2*	This study
Sinocyclocheilus anshuiensis	Tibetan cavefish	*rh1-2*	XM_016497364.1
Sinocyclocheilus grahami	Golden-line barbel	*rh1-2*	XM_016233062.1
Sinocyclocheilus rhinocerous	Tibetan cavefish	*rh1-2*	XM_016524871.1
Scopelarchus analis	Pearleye	*rh1A*	EF517404.1
Scopelarchus analis	Pearleye	*rh1B*	EF517405.1
Gallus gallus	Chicken	*rh2*	45382766
Latimeria chalumnae	Coelacanth	*rh2*	4836680-4836684
Oryzias latipes	Japanese medaka	*rh2*	86198067
Danio rerio	Zebrafish	*rh2-1*	42476236

Table S2. Results of random sites (PAML) analyses on subsets of the vertebrate *rh1* gene tree.

Tree[1]	Model and Partition	np	ln *L*	*κ*	Parameters[2]			Null	LRT	df	*p*
					ω_0/p	ω_1/q	ω_2/ω_p				
Vert	M0	281	-49103.07	1.90	0.07			n/a			
	M1a	282	-48490.32	1.99	0.06 (92.7%)	1 (7.3%)		M0	1225.50	1	**0.0000**
	M2a	284	-48490.32	1.99	0.06 (92.7%)	1 (4.2%)	1 (3.1%)	M1a	0.00	2	1.0000
	M3	285	-47211.50	1.87	0.01 (54.8%)	0.11 (35.5%)	0.37 (9.7%)	M0	3783.13	4	**0.0000**
	M7	282	-47137.43	1.87	0.383	3.014		n/a			
	M8a	283	-47124.15	1.88	0.420	4.196	1 (0.8%)	n/a			
	M8	284	-47124.15	1.88	0.420	4.196	1 (0.8%)	M7	26.56	2	**0.0000**
								M8a	0.00	1	1.0000
Acti	M0	221	-35771.32	1.99	0.08			n/a			
	M1a	222	-35181.81	2.10	0.06 (92.3%)	1 (7.7%)		M0	1179.02	1	**0.0000**
	M2a	224	-35181.81	2.10	0.06 (92.3%)	1 (3.6%)	1 (4.1%)	M1a	0.00	2	1.0000
	M3	225	-34324.43	1.97	0.01 (56.5%)	0.12 (33.9%)	0.41 (9.6%)	M0	2893.79	4	**0.0000**
	M7	222	-34262.33	1.97	0.32	2.35		n/a			
	M8a	223	-34245.81	1.97	0.36	3.27	1 (0.8%)	n/a			
	M8	224	-34245.81	1.97	0.36	3.27	1 (0.8%)	M7	33.04	2	**0.0000**
								M8a	0.00	1	0.9984
rh1-2	M0	21	-3541.57	2.48	0.09			n/a			
	M1a	22	-3500.77	2.63	0.03 (89.4%)	1 (10.6%)		M0	81.60	1	**0.0000**
	M2a	24	-3500.77	2.63	0.03 (89.4%)	1 (7.9%)	1 (2.7%)	M1a	0.00	2	1.0000
	M3	25	-3488.86	2.46	0.00 (72.5%)	0.32 (26.9%)	3.08 (0.6%)	M0	105.41	4	**0.0000**
	M7	22	-3491.58	2.50	0.13	1.10		n/a			
	M8a	23	-3491.00	2.50	0.16	1.70	1 (2%)	n/a			
	M8	24	-3489.65	2.49	0.15	1.41	3.29 (0.5%)	M7	3.87	2	0.1442
								M8a	2.70	1	0.1004

[1]The full vertebrate *rh1* (Vert) and gene trees pruned to contain only actinopterygian rhodopsins (Acti) and only *rh1-2*.

[2]ω values of each site class are shown for models M0-M3 (ω_0– ω_2) with the proportion of each site class in parentheses. For M7-M8, the shape parameters, p and q, which describe the beta distribution are listed. In addition, the ω value for the positively selected site class (ω_p, with the proportion of sites in parentheses) is shown for M8a (where ω_p is constrained to equal one) and M8.

Abbreviations—**np**, number of parameters; ***ln*L**, *ln* Likelihood; **κ**, transition/transversion ratio; **LRT**, likelihood ratio test statistic; **df**, degrees of freedom; ***p***, *p*-value; **n/a**, not applicable.

Table S3. Results of branch and branch-site (PAML) analyses with the branch leading to the *rh1-2* clade placed into the foreground.

Partition	Model	np	ln *L*	*κ*	Parameters[1]				LRT	df	*p*
					ω_0	ω_1	ω_{2a}	ω_{2b}			
M0	Null	221	-35771.32	1.99	0.08						
Branch	Alt	222	-35770.90	1.99	B: 0.09 F: 0.06				0.84	1	0.3607
Branch-site	Null	223	-35175.73	2.10	B: 0.06 F: 0.06 (85.4%)	B: 1 F: 1 (7.2%)	B: 0.06 F: 1 (6.8%)	B: 1 F: 1 (0.6%)			
Branch-site	Alt	224	-35174.10	2.10	B: 0.06 F: 0.06 (88.1%)	B: 1 F: 1 (7.5%)	B: 0.06 F: 31.22 (4%)	B: 1 F: 31.22 (0.4%)	3.25	1	0.0713

[1]ω values of each site class are shown with the proportion of each site class in parentheses. B and F refer to the background and foreground partitions.
Abbreviations—**np**, number of parameters; **ln *L***, *ln* Likelihood; ***κ***, transition/transversion ratio; **LRT**, likelihood ratio test statistic; **df**, degrees of freedom; ***p***, *p*-value; **n/a**, not applicable.

Table S4. Results of branch, branch-site, and clade model C (PAML) analyses with the *rh1-2* clade placed into the foreground.

Partition	Model	np	ln *L*	*κ*	Parameters1				LRT	df	*p*
					ω_0	ω_1	ω_{2a}/ω_d	ω_{2b}			
M0	Null	221	-35771.32	1.99	0.08						
Branch	Alt	222	-35771.23	1.99	B: 0.08 F: 0.07				0.18	1	0.6735
Branch-site	Null	223	-35150.11	2.10	B: 0.06 F: 0.06 (85.8%)	B: 1 F: 1 (7.2%)	B: 0.06 F: 1 (6.5%)	B: 1 F: 1 (0.5%)			
Branch-site	Alt	224	-35150.11	2.10	B: 0.06 F: 0.06 (85.8%)	B: 1 F: 1 (7.2%)	B: 0.06 F: 1 (6.5%)	B: 1 F: 1 (0.5%)	0.00	1	0.9901
M2a_rel	Null	224	-34416.38	2.03	0.01 (60.8%)	1 (3.1%)	0.16 (36.1%)				
CmC	Alt	225	-34416.36	2.03	B: 0.01 F: 0.01 (60.8%)	B: 1 F: 1 (3.1%)	B: 0.16 F: 0.16 (36.1%)		0.04	1	0.8437

[1]ω values of each site class are shown with the proportion of each site class in parentheses. B and F refer to the background and foreground partitions.
Abbreviations—**np**, number of parameters; **ln *L***, *ln* Likelihood; ***κ***, transition/transversion ratio; **LRT**, likelihood ratio test statistic; **df**, degrees of freedom; ***p***, *p*-value; **n/a**, not applicable

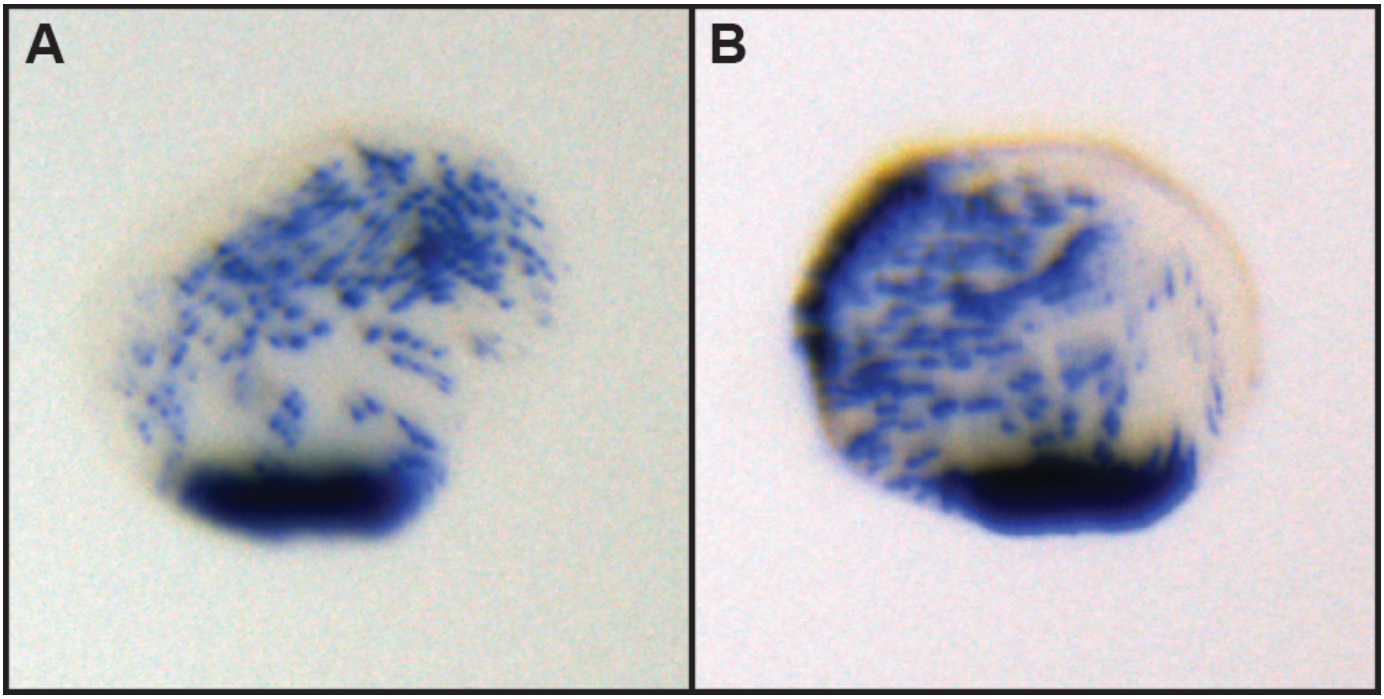

Figure S1. *In situ* hybridization of *rh1* in 3 dpf zebrafish embryos. Retinas from 3 dpf embryos were stained with the same 700 bp *rh1* probe used in all other experiments in this study both (A) with and (B) without the addition of full-length *rh1-2* blocking RNA, present at double the concentration of the rh1 probe. No significant difference in staining was detected.

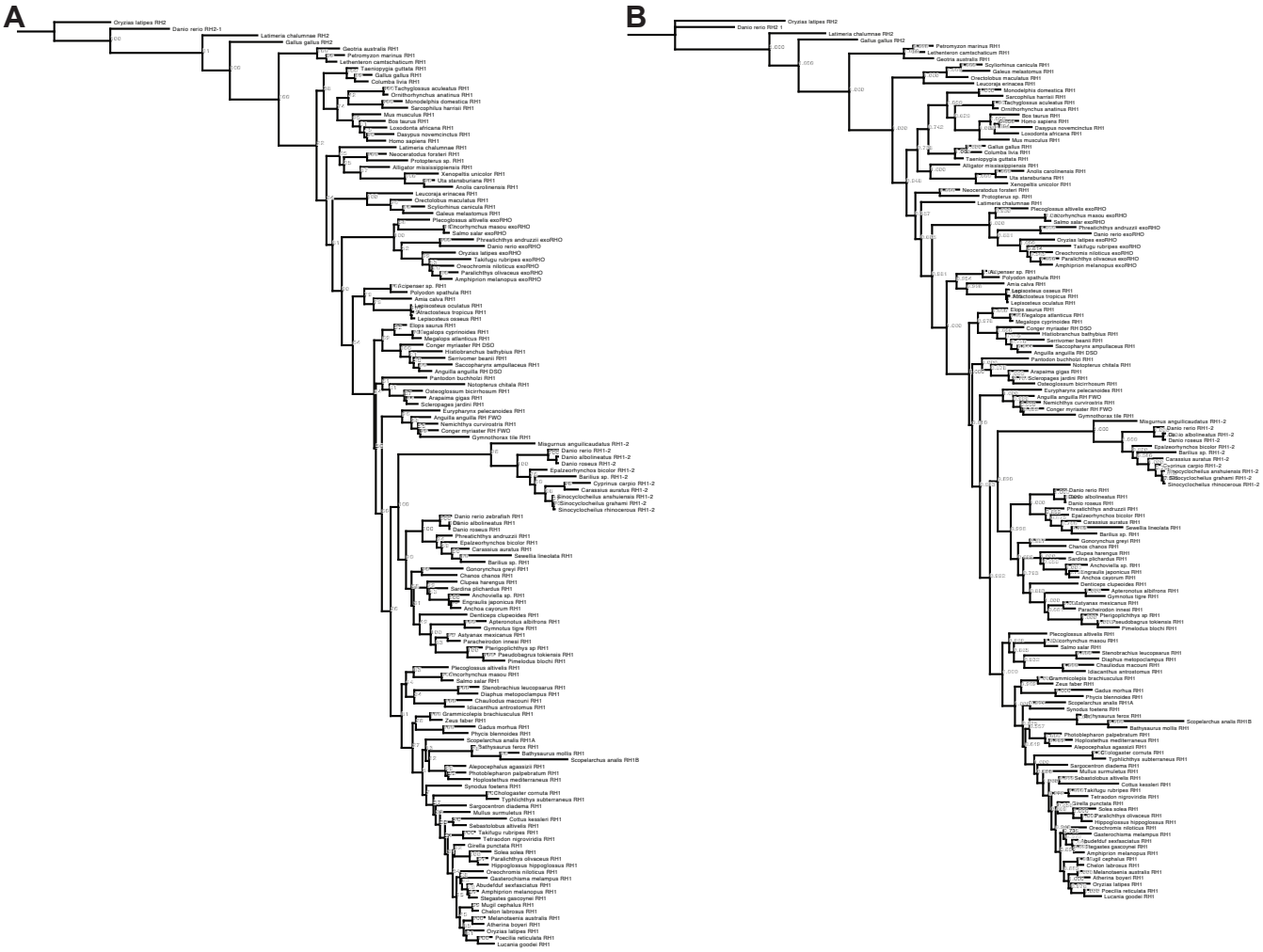

Figure S2. Detailed maximum-likelihood (A) and Bayesian phylogeny (B) of vertebrate rhodopsin genes. In both cases, high support was recovered for the placement of the *rh1-2* gene family as the sister group to Ostarioclupeomorpha. Several *rh2* opsin sequences were used as outgroups.

Table S1. List of sequences used in the phylogenetic and molecular evolutionary analyses of *rh1* genes.

Species Name	Common Name[1]	Gene	Accession/GI Number
Amphiprion melanopus	Fire clownfish	*exorh*	HM107820.1
Danio rerio	Zebrafish	*exorh*	71534272
Oncorhynchus masou	Masu salmon	*exorh*	478430872
Oreochromis niloticus	Nile tilapia	*exorh*	XM003438995.1
Oryzias latipes	Japanese medaka	*exorh*	XM004070540.1
Paralichthys olivaceus	Olive flounder	*exorh*	HM107825.1
Phreatichthys andruzzii	Cavefish	*exorh*	GQ404491.1
Plecoglossus altivelis	Ayu	*exorh*	28201134
Salmo salar	Atlantic salmon	*exorh*	185133057
Takifugu rubripes	Pufferfish	*exorh*	76362825
Anguilla anguilla	European eel	*rh1dso*	L78008.1
Conger myriaster	Whitespotted conger	*rh1dso*	12583666
Anguilla anguilla	European eel	*rh1fwo*	L78007.1
Conger myriaster	Whitespotted conger	*rh1fwo*	12583664
Abudefduf sexfasciatus	Scissortail sergeant	*rh1*	HQ286548.1
Acipenser sp.	Sturgeon	*rh1*	AF137206.1
Alepocephalus agassizii	Slickhead	*rh1*	JN544545.1
Alligator mississippiensis	American alligator	*rh1*	U23802.1
Amia calva	Bowfin	*rh1*	AF137208.1
Amphiprion melanopus	Fire clownfish	*rh1*	HM107824.1
Anchoa cayorum	Key anchovy marine	*rh1*	This study
Anchoviella sp.	Freshwater anchovy	*rh1*	This study
Anolis carolinensis	Carolina anole	*rh1*	XM003224879.1
Apteronotus albifrons	Black ghost knifefish	*rh1*	JN230983.1
Arapaima gigas	Arapaima	*rh1*	JN230972.1
Astyanax mexicanus	Mexican tetra	*rh1*	U12328.1
Atherina boyeri	Big-scale sand smelt	*rh1*	Y18676.1
Atractosteus tropicus	Tropical gar	*rh1*	JN230970.1
Barilius sp.	Barilius	*rh1*	This study
Bathysaurus ferox	Deepsea lizardfish	*rh1*	JN412585.1
Bathysaurus mollis	Highfin lizardfish	*rh1*	JN412586.1
Bos taurus	Cow	*rh1*	NM001014890.1
Carassius auratus	Golfish	*rh1*	L11863.1
Chanos chanos	Milfish	*rh1*	JN230981.1
Chauliodus macouni	Pacific viperfish	*rh1*	EU407250.1
Chelon labrosus	Thicklip grey mullet	*rh1*	Y18669.1
Chologaster cornuta	Swampfish	*rh1*	HQ729684.1
Clupea harengus	Atlantic herring	*rh1*	XM_012826141.1
Columba livia	Pigeon	*rh1*	4887218-4887219
Cottus kessleri	Kesslers sculpin	*rh1*	L42953.1
Danio albolineatus	Pearl danio	*rh1*	JQ614122.1

Danio rerio	Zebrafish	*rh1*	18859316:
Danio roseus	Rose danio	*rh1*	JQ614148.1
Dasypus novemcinctus	Armadillo	*rh1*	XM004477246.1
Denticeps clupeoides	Denticle herring	*rh1*	JN230976.1
Diaphus metopoclampus	Spothead lantern fish	*rh1*	JN544536.1
Elops saurus	Ladyfish	*rh1*	JN230971.1
Engraulis japonicus	Japanese anchovy	*rh1*	AB731902.1
Epalzeorhynchos bicolor	Redtailed black shark	*rh1*	HQ286332.1
Eurypharynx pelecanoides	Pelican eel	*rh1*	JN544544.1
Gadus morhua	Atlantic cod	*rh1*	AF385832.1
Galeus melastomus	Blackmouth catshark	*rh1*	Y17586.1
Gallus gallus	Chicken	*rh1*	NM001030606.1
Gasterochisma melampus	Butterfly kingfish	*rh1*	DQ882021.1
Geotria australis	Pouched lamprey	*rh1*	AY366493.1
Girella punctata	Largescale blackfish	*rh1*	AB158262.3
Gnorhynchus greyi	Beaked salmon	*rh1*	EU409632
Grammicolepis brachiusculus	Thorny tinselfish	*rh1*	EU637964.1
Gymnothorax tile	Moray eel	*rh1*	This study
Gymnotus tigre	Tiger knifefish	*rh1*	This study
Hippoglossus hippoglossus	Atlantic halibut	*rh1*	AF156265.1
Histiobranchus bathybius	Deepwater arrowtooth eel	*rh1*	JN544542.1
Homo sapiens	Human	*rh1*	169808383
Hoplostethus mediterraneus	Mediterranean slimehead	*rh1*	JN412583.1
Idiacanthus antrostomus	Pacific blackdragon	*rh1*	EU407249.1
Latimeria chalumnae	Coelacanth	*rh1*	4836673-4836677
Lepisosteus oculatus	Spotted gar	*rh1*	This study
Lepisosteus osseus	Longnose gar	*rh1*	AF137207.1
Lethenteron camtschaticum	Artic lamprey	*rh1*	46917273
Leucoraja erinacea	Little skate	*rh1*	U81514.1
Loxodonta africana	Elephant	*rh1*	344275992
Lucania goodei	Bluefin killifish	*rh1*	AY296738.1
Megalops atlanticus	Atlantic tarpon	*rh1*	AY158050
Megalops cyprinoides	Indo-Pacific tarpon	*rh1*	This study
Melanotaenia australis	Western rainbowfish	*rh1*	FJ940704.1
Monodelphis domestica	Short-tailed opossum	*rh1*	XM001366188.1
Mugil cephalus	Flathead mullet	*rh1*	4210736
Mullus surmuletus	Striped red mullet	*rh1*	4210732
Mus musculus	Mouse	*rh1*	NM_145383.1
Nemichthys curvirostris	Boxer snipe eel	*rh1*	This study
Neoceratodus forsteri	Lungfish	*rh1*	EF526295.1
Notopterus chitala	Clown knifefish	*rh1*	This study
Oncorhynchus masou	Masu salmon	*rh1*	478430870
Orectolobus maculatus	Spotted wobbegong	*rh1*	JX534163.1
Oreochromis niloticus	Niles tilapia	*rh1*	348502996
Ornithorhynchus anatinus	Platypus	*rh1*	NM001127627.1

Oryzias latipes	Japanese medaka	*rh1*	66796119
Osteoglossum bicirrhosum	Silver arowana	*rh1*	This study
Pantodon buchholzi	Freshwater butterflyfish	*rh1*	AF137210.1
Paracheirodon innesi	Neon tetra	*rh1*	84095053
Paralichthys olivaceus	Olive flounder	*rh1*	HQ413772.1
Petromyzon marinus	Sea lamprey	*rh1*	1513320-1513324
Photoblepharon palpebratum	Eyelightfish	*rh1*	EU637993.1
Phreatichthys andruzzii	Cavefish	*rh1*	JQ413240.1
Phycis blennoides	Greater forkbeard	*rh1*	JN412579.1
Pimelodus blochim	Blochs catfish	*rh1*	This study
Plecoglossus altivelis	Ayu	*rh1*	19912833
Poecilia reticulata	Guppy	*rh1*	DQ912024.1
Polyodon spathula	American paddlefish	*rh1*	AF369050.1
Protopterus sp.	African lungfish	*rh1*	AF369054.1
Pseudobagrus tokiensis	Balgrid	*rh1*	FJ197075.1
Pterigoplichthys sp.	Armored catfish	*rh1*	This study
Saccopharynx ampullaceus	Gulper eel	*rh1*	This study
Salmo salar	Atlantic salmon	*rh1*	185133085
Sarcophilus harrisii	Tasmian devil	*rh1*	395516643
Sardina pilchardus	Sardine	*rh1*	Y18677.1
Sargocentron diadema	Crown squirrelfish	*rh1*	U57537.1
Scleropages jardini	Gulf saratoga	*rh1*	This study
Scyliorhinus canicula	Small-spotted catshark	*rh1*	3256019
Sebastolobus altivelis	Longspine thornyhead	*rh1*	DQ490124.1
Serrivomer beanii	Sawtooth eel	*rh1*	This study
Sewellia lineolata	Tiger hillstream loach	*rh1*	This study
Solea solea	Common sole	*rh1*	4210866
Stegastes gascoynei	Coral Sea gregory damselfish	*rh1*	HQ286557.1
Stenobrachius leucopsarus	Northern lampfish	*rh1*	EU407251.1
Synodus foetens	Inshore lizardfish	*rh1*	JN231001.1
Tachyglossus aculeatus	Echidna	*rh1*	398018454
Taeniopya guttata	Zebra finch	*rh1*	115529257
Takifugu rubripes	Pufferfish	*rh1*	118344635
Tetraodon nigroviridis	Green spotted puffer	*rh1*	AJ293018.1
Typhlichthys subterraneus	Southern cavefish	*rh1*	HQ729699.1
Uta stansburiana	Side-blotched lizard	*rh1*	DQ100323.1
Xenopeltis unicolor	Sunbeam snake	*rh1*	FJ497233.1
Zeus faber	John dory	*rh1*	Y14484.1
Barilius sp.	Barilius	*rh1-2*	This study
Carassius auratus	Goldfish	*rh1-2*	This study
Cyprinus carpio	Common carp	*rh1-2*	Extracted from genome
Danio albolineatus	Pearl danio	*rh1-2*	HQ286328
Danio rerio	Zebrafish	*rh1-2*	HQ286326
Danio roseus	Rose danio	*rh1-2*	HQ286327
Epalzeorhynchos bicolor	Redtailed black shark	*rh1-2*	HQ286329

Misgurnus anguilicaudatus	Dojo loach	*rh1-2*	This study
Sinocyclocheilus anshuiensis	Tibetan cavefish	*rh1-2*	XM_016497364.1
Sinocyclocheilus grahami	Golden-line barbel	*rh1-2*	XM_016233062.1
Sinocyclocheilus rhinocerous	Tibetan cavefish	*rh1-2*	XM_016524871.1
Scopelarchus analis	Pearleye	*rh1A*	EF517404.1
Scopelarchus analis	Pearleye	*rh1B*	EF517405.1
Gallus gallus	Chicken	*rh2*	45382766
Latimeria chalumnae	Coelacanth	*rh2*	4836680-4836684
Oryzias latipes	Japanese medaka	*rh2*	86198067
Danio rerio	Zebrafish	*rh2-1*	42476236

Table S2. Results of random sites (PAML) analyses on subsets of the vertebrate *rh1* gene tree.

Tree[1]	Model and Partition	np	ln *L*	κ	Parameters[2]			Null	LRT	df	*p*
					ω_0/p	ω_1/q	ω_2/ω_p				
Vert	M0	281	-49103.07	1.90	0.07			n/a			
	M1a	282	-48490.32	1.99	0.06 (92.7%)	1 (7.3%)		M0	1225.50	1	**0.0000**
	M2a	284	-48490.32	1.99	0.06 (92.7%)	1 (4.2%)	1 (3.1%)	M1a	0.00	2	1.0000
	M3	285	-47211.50	1.87	0.01 (54.8%)	0.11 (35.5%)	0.37 (9.7%)	M0	3783.13	4	**0.0000**
	M7	282	-47137.43	1.87	0.383	3.014		n/a			
	M8a	283	-47124.15	1.88	0.420	4.196	1 (0.8%)	n/a			
	M8	284	-47124.15	1.88	0.420	4.196	1 (0.8%)	M7	26.56	2	**0.0000**
								M8a	0.00	1	1.0000
Acti	M0	221	-35771.32	1.99	0.08			n/a			
	M1a	222	-35181.81	2.10	0.06 (92.3%)	1 (7.7%)		M0	1179.02	1	**0.0000**
	M2a	224	-35181.81	2.10	0.06 (92.3%)	1 (3.6%)	1 (4.1%)	M1a	0.00	2	1.0000
	M3	225	-34324.43	1.97	0.01 (56.5%)	0.12 (33.9%)	0.41 (9.6%)	M0	2893.79	4	**0.0000**
	M7	222	-34262.33	1.97	0.32	2.35		n/a			
	M8a	223	-34245.81	1.97	0.36	3.27	1 (0.8%)	n/a			
	M8	224	-34245.81	1.97	0.36	3.27	1 (0.8%)	M7	33.04	2	**0.0000**
								M8a	0.00	1	0.9984
rh1-2	M0	21	-3541.57	2.48	0.09			n/a			
	M1a	22	-3500.77	2.63	0.03 (89.4%)	1 (10.6%)		M0	81.60	1	**0.0000**
	M2a	24	-3500.77	2.63	0.03 (89.4%)	1 (7.9%)	1 (2.7%)	M1a	0.00	2	1.0000
	M3	25	-3488.86	2.46	0.00 (72.5%)	0.32 (26.9%)	3.08 (0.6%)	M0	105.41	4	**0.0000**
	M7	22	-3491.58	2.50	0.13	1.10		n/a			
	M8a	23	-3491.00	2.50	0.16	1.70	1 (2%)	n/a			
	M8	24	-3489.65	2.49	0.15	1.41	3.29 (0.5%)	M7	3.87	2	0.1442
								M8a	2.70	1	0.1004

[1]The full vertebrate *rh1* (Vert) and gene trees pruned to contain only actinopterygian rhodopsins (Acti) and only *rh1-2*.

[2]ω values of each site class are shown for models M0-M3 (ω_0– ω_2) with the proportion of each site class in parentheses. For M7-M8, the shape parameters, p and q, which describe the beta distribution are listed. In addition, the ω value for the positively selected site class (ω_p, with the proportion of sites in parentheses) is shown for M8a (where ω_p is constrained to equal one) and M8.

Abbreviations—**np**, number of parameters; ***ln*L**, *ln* Likelihood; **κ**, transition/transversion ratio; **LRT**, likelihood ratio test statistic; **df**, degrees of freedom; ***p***, *p*-value; **n/a**, not applicable.

Table S3. Results of branch and branch-site (PAML) analyses with the branch leading to the *rh1-2* clade placed into the foreground.

Partition	Model	np	ln *L*	*κ*	Parameters[1]				LRT	df	*p*
					ω_0	ω_1	ω_{2a}	ω_{2b}			
M0	Null	221	-35771.32	1.99	0.08						
Branch	Alt	222	-35770.90	1.99	B: 0.09 F: 0.06				0.84	1	0.3607
Branch-site	Null	223	-35175.73	2.10	B: 0.06 F: 0.06 (85.4%)	B: 1 F: 1 (7.2%)	B: 0.06 F: 1 (6.8%)	B: 1 F: 1 (0.6%)			
Branch-site	Alt	224	-35174.10	2.10	B: 0.06 F: 0.06 (88.1%)	B: 1 F: 1 (7.5%)	B: 0.06 F: 31.22 (4%)	B: 1 F: 31.22 (0.4%)	3.25	1	0.0713

[1]ω values of each site class are shown with the proportion of each site class in parentheses. B and F refer to the background and foreground partitions.
Abbreviations—**np**, number of parameters; **ln *L***, *ln* Likelihood; ***κ***, transition/transversion ratio; **LRT**, likelihood ratio test statistic; **df**, degrees of freedom; ***p***, *p*-value; **n/a**, not applicable.

Table S4. Results of branch, branch-site, and clade model C (PAML) analyses with the *rh1-2* clade placed into the foreground.

Partition	Model	np	ln *L*	*κ*	Parameters1				LRT	df	*p*
					ω_0	ω_1	ω_{2a}/ω_d	ω_{2b}			
M0	Null	221	-35771.32	1.99	0.08						
Branch	Alt	222	-35771.23	1.99	B: 0.08 F: 0.07				0.18	1	0.6735
Branch-site	Null	223	-35150.11	2.10	B: 0.06 F: 0.06 (85.8%)	B: 1 F: 1 (7.2%)	B: 0.06 F: 1 (6.5%)	B: 1 F: 1 (0.5%)			
Branch-site	Alt	224	-35150.11	2.10	B: 0.06 F: 0.06 (85.8%)	B: 1 F: 1 (7.2%)	B: 0.06 F: 1 (6.5%)	B: 1 F: 1 (0.5%)	0.00	1	0.9901
M2a_rel	Null	224	-34416.38	2.03	0.01 (60.8%)	1 (3.1%)	0.16 (36.1%)				
CmC	Alt	225	-34416.36	2.03	B: 0.01 F: 0.01 (60.8%)	B: 1 F: 1 (3.1%)	B: 0.16 F: 0.16 (36.1%)		0.04	1	0.8437

[1]ω values of each site class are shown with the proportion of each site class in parentheses. B and F refer to the background and foreground partitions.
Abbreviations—**np**, number of parameters; **ln *L***, *ln* Likelihood; ***κ***, transition/transversion ratio; **LRT**, likelihood ratio test statistic; **df**, degrees of freedom; ***p***, *p*-value; **n/a**, not applicable